Improved consistency between the modelling of ocean optics, biogeochemistry and physics, and its impact on the North-West European Shelf seas

Jozef Skakala[1,1], Jorn Bruggeman[2,2], David Andrew Ford[3,3], Sarah L Wakelin[4,4], Anıl Akpınar[4,4], Tom Hull[5,5], Jan Kaiser[6,6], Benjamin Roger Loveday[1,1], Charlotte Anne June Williams[4,4], and Stefano Ciavatta[7,7]

[1]Plymouth Marine Laboratory
[2]PML
[3]Met Office
[4]National Oceanography Centre
[5]Centre for Environment, Fisheries and Aquaculture Science
[6]University of East Anglia
[7]Plymouth Marine Laboratory/National Centre for Earth Observation

November 30, 2022

Abstract

We use a recently developed spectrally resolved bio-optical module to better represent the interaction between the incoming irradiance and the heat fluxes in the upper ocean within the (pre-)operational physical-biogeochemical model on the North-West European (NWE) Shelf. The module attenuates light based on the simulated biogeochemical tracer concentrations, and thus introduces a two-way coupling between the biogeochemistry and physics. We demonstrate that in the late spring-summer the two-way coupled model heats up the upper oceanic layer, shallows the mixed layer depth and influences the mixing in the upper ocean. The increased heating in the upper oceanic layer reduces the convective mixing and improves by ~5 days the timing of the late phytoplankton bloom of the ecosystem model. This improvement is relatively small compared with the existing model bias in bloom timing, but sufficient to have a visible impact on model skill. We show that the changes to the model temperature and salinity introduced by the module have mixed impact on the physical model skill, but the skill can be improved by assimilating the observations of temperature, salinity and chlorophyll into the model. However, in the situations where we improved the simulation of temperature, either via the bio-optical module, or via assimilation of temperature and salinity, we have shown that we also improved the simulated oxygen concentration as a result of the changes in the simulated air-sea gas flux. Overall, comparing different 1-year experiments showed that the best model skill is achieved with joint physical-biogeochemical assimilation into the two-way coupled model.

Highlights

Improved consistency between the modelling of ocean optics, biogeochemistry and physics, and its impact on the North-West European Shelf seas

Jozef Skákala, Jorn Bruggeman, David Ford, Sarah Wakelin, Anıl Akpınar, Tom Hull, Jan Kaiser, Benjamin R. Loveday, Charlotte A.J. Williams, Stefano Ciavatta

- We established two-way coupling between biogeochemistry and physics.
- We assessed the impact of the coupling in free and assimilative experiments.
- The two-way coupling improves the simulated biogeochemistry on the NWE Shelf.
- We recommend to implement this development into the operational system.

Improved consistency between the modelling of ocean optics, biogeochemistry and physics, and its impact on the North-West European Shelf seas

Jozef Skákala[a,b], Jorn Bruggeman[a], David Ford[c], Sarah Wakelin[d], Anıl Akpınar[d], Tom Hull[e,f], Jan Kaiser[f], Benjamin R. Loveday[g], Charlotte A.J. Williams[d], Stefano Ciavatta[a,b]

[a]*Plymouth Marine Laboratory, Prospect Place, The Hoe, Plymouth, PL1 3DH, United Kingdom*
[b]*National Centre for Earth Observation, Prospect Place, The Hoe, Plymouth, PL1 3DH, United Kingdom*
[c]*Met Office, FitzRoy Road, Exeter, EX1 3PB, United Kingdom*
[d]*National Oceanography Centre, Joseph Proudman Building, 6 Brownlow Street, Liverpool, L3 5DA, United Kingdom*
[e]*Centre for Environment, Fisheries and Aquaculture Science, Lowesoft, NR33 0HT, United Kingdom*
[f]*Centre for Ocean and Atmospheric Science, University of East Anglia, Norwich, NR4 7TJ, United Kingdom*
[g]*Innoflair UG, Richard-Wagner-Weg 35, Darmstadt, 64287, Germany*

Abstract

We use a recently developed spectrally resolved bio-optical module to better represent the interaction between the incoming irradiance and the heat fluxes in the upper ocean within the (pre-)operational physical-biogeochemical model on the North-West European (NWE) Shelf. The module attenuates light based on the simulated biogeochemical tracer concentrations, and thus introduces a two-way coupling between the biogeochemistry and physics. We demonstrate that in the late spring-summer the two-way coupled model heats up the upper oceanic layer, shallows the mixed layer depth and influences the mixing in the upper ocean. The increased heating in the upper oceanic layer reduces the convective mixing and improves by ∼5 days the timing of the late phytoplankton bloom of the ecosystem model. This improvement is relatively small compared with the existing model bias in bloom timing, but sufficient to have a visible impact on model skill. We show that the changes to the model temperature and salinity introduced by the module have mixed

impact on the physical model skill, but the skill can be improved by assimilating the observations of temperature, salinity and chlorophyll concentrations into the model. However, in the situations where we improved the simulation of temperature, either via the bio-optical module, or via assimilation of temperature and salinity, we have shown that we also improved the simulated oxygen concentration as a result of the changes in the simulated air-sea gas flux. Overall, comparing different 1-year experiments showed that the best model skill is achieved with joint physical-biogeochemical assimilation into the two-way coupled model.

Keywords: two-way coupled physical-biogeochemical model, ocean chlorophyll concentration, sea surface temperature, phytoplankton spring bloom, North-West European Shelf (10E-10W, 40N-68N), data assimilation

1. Introduction

Physical-biogeochemical ocean models are an essential element in monitoring and forecasting of global and shelf-sea ecosystem indicators ([1, 2]). However, coupled physical-biogeochemical marine modelling is a complex undertaking and a common way to simplify coupled models is to neglect the impact of the biogeochemical model state on physics ([3, 2]). Although marine ecosystem models often neglect the coupling from the biogeochemical model state to physics, there are number of established mechanisms through which biogeochemistry influences physics and climate ([4, 1, 2]): (i) marine ecosystems play an essential part in the carbon cycle through biological and microbial carbon pump, influencing atmospheric carbon concentrations and the Earth surface temperature, (ii) phytoplankton influences oceanic albedo (e.g. [5]) having an overall impact on the radiative terms and Earth energy budget, (iii) some biogeochemical tracers influence light attenuation, modifying the short-wave heat fluxes in the water column and therefore ocean stratification ([6, 7, 8, 9, 10, 11, 12, 13, 14]), and (iv) marine ecosystems have an impact on cloud condensation nuclei through the production of dimethyl sulfide (DMS, [15, 16, 17, 18]), or more directly via bubble formation ([19]). The size of life's impact on Earth's physics has been subject to much debate ([2]), often in connection with "the Gaia hypothesis" ([20, 21]), which proposes that life plays a central role in regulating climate.

For coupled physical-biogeochemical marine models the main source of impact of ecosystems on physics is through the absorption and backscatter-

ing of short-wave radiation by some biogeochemical substances in the sea water (e.g. [10]). The presence of optically active tracers, such as chlorophyll, suspended particulate matter (SPM), or colored dissolved organic matter (CDOM), in the oceanic upper layer increases light attenuation near the oceanic surface, warms the sea temperature in the upper ocean, which typically influences the mixing in the upper oceanic layer (e.g. [6]), e.g. shallowing the thermocline and the mixed layer depth (MLD). The changes to the vertical mixing can in turn impact the biogeochemical model, by influencing the nutrient concentrations and growth conditions in the upper ocean.

In this work we focus on the Copernicus Marine Environmental Monitoring Service (CMEMS) operational system for the North-West European (NWE) Shelf biogeochemistry, which is of a substantial societal benefit, as the NWE Shelf is a key region for fisheries, and an important contributor to the global carbon cycle ([22, 23, 24]). The presently used physical-biogeochemical operational model for the NWE Shelf is the marine physical model Nucleus for European Modelling of the Ocean (NEMO, [25]) coupled through the Framework for Aquatic Biogeochemical Models (FABM, [26, 27]) to the European Regional Seas Ecosystem Model (ERSEM, [28, 29, 30]). NEMO-FABM-ERSEM drives its physics and biogeochemistry by two separate irradiance modules: (i) the physical model calculates heat fluxes from the incoming net short-wave radiation (SWR) split into two wavebands, the 400-700nm visible band reduced through attenuation obtained from a monthly climatology of a satellite surface K_d product at 490nm wavelength (European Space Agency product version 2.0, https://www.esa-oceancolour- cci.org/), and the UV/infrared band reduced with a preset attenuation with an e-folding scale of 0.35m, (ii) the biogeochemical model reduces incoming photosynthetic active radiation (PAR) by taking into account both absorption and backscattering by the sea water and the simulated Phytoplankton Functional Types (PFTs), and also by including absorption by Particulate Organic Matter (POM), CDOM and sediment represented by an external satellite product (for details see [29, 31]). The presently used scheme means that, although some impact of biogeochemical tracers on the physical model is implicitly included in the 490nm K_d satellite climatology, there is no feedback from the biogeochemical model state to the simulated physics.

In [31] we implemented into ERSEM a stand-alone bio-optical module (based on OASIM, [32, 33, 34]), that resolves irradiance spectrally and splits the irradiance into diffuse and direct streams ([35]). The module then propagates irradiance through the water column, based on attenuation by sea water

and the biogeochemical substances in the water. The new module drove only the biogeochemical part of the coupled NEMO-FABM-ERSEM model, substantially improving the underwater irradiance, but without a major impact on the ERSEM model skill on the NWE Shelf ([31]). This version of NEMO-FABM-ERSEM model will be used in the present study as a reference run and will be called a "one-way coupled model". In this work we expand the development implemented in [31] by using the bio-optical module to drive both the biogeochemistry and the physics (i.e. heating by light absorption). Since the physical heat fluxes will be driven by the underwater irradiance that is attenuated by biogeochemical substances, the module establishes an important feedback from the biogeochemical model to physics. We will further call this new implementation a "two-way coupled model", to distinguish it from the "one-way coupled" reference run.

This work aims at answering two main questions: (i) What is the size of the biogeochemical impact on the marine physics within the NWE Shelf? (ii) Does the impact of the spectrally resolved bio-optical module on physics lead to more internally consistent ecosystem dynamics on the NWE Shelf, and hence, an improvement in the operational biogeochemical model skill? Those two questions are answered both in the context of free simulations and also in the context of (physical, biogeochemical, coupled) assimilative runs. The second question is particularly relevant: It has been established that NEMO-FABM-ERSEM displays on the NWE Shelf late and intense spring blooms ([31, 36]). Since a spring bloom is a major ecosystem driver ([37, 38]), the simulated late blooms severely limit the ecosystem model skill ([31, 36]). Although many factors can influence the bloom timing (including biological drivers, such as zooplankton grazing, e.g. [39]), one of the leading hypotheses for how phytoplankton blooms are triggered in the North Atlantic is based on the interplay between PAR and an effective mixing depth (the critical turbulence hypothesis, [40, 41]), i.e. the bloom sets in when the effective mixing depth becomes fully contained within the euphotic layer ([42]). Within the scope of the critical turbulence hypothesis, the delay in bloom timing could then be explained by multiple components within the physical-biogeochemical coupled model: (a) atmospheric wind stress forcing, (b) model upper-ocean mixing scheme, (c) vertical stratification (thermocline and pycnocline), (d) incoming surface PAR, (e) underwater light attenuation, (f) the phytoplankton growth response to light (e.g. model parameters, such as P-I curves, maximum PFT chlorophyll-to-carbon ratios). In [31] we have addressed to a varying degree the points (d) and (e) without a significant

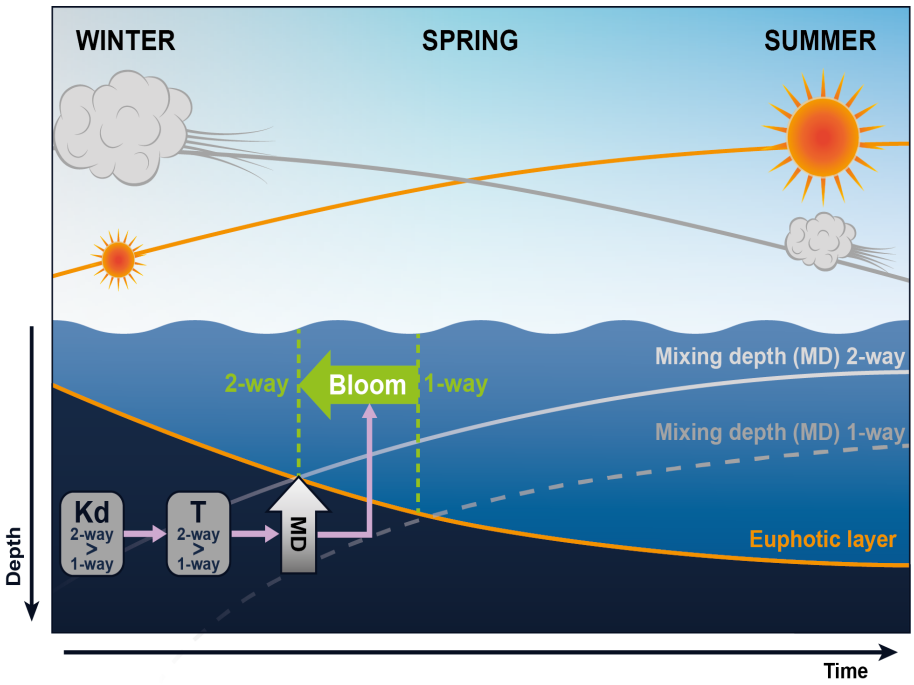

Figure 1: A schematic representation of the hypothesis about the impact of the two-way coupled model on the timing of the simulated bloom.

impact on the bloom timing. However, [31] observed that attenuation of light based on the satellite K_d product for the 490 nm wavelength is most likely an underestimate of the total PAR absorbed in the upper oceanic layer. Calculating heat fluxes using the bio-optical module is therefore expected to produce extra heat in the upper oceanic layer (Fig.5 of [31]), which is thought to shallow the MLD, but it can also reduce turbulent convective mixing near the oceanic surface ([43, 44]). The hypothesis tested in this work (see Fig.1) is that the reduced convective mixing can lead to a shallower turbulent mixing depth and help trigger an earlier phytoplankton bloom, as suggested by the critical turbulence hypothesis ([40, 44]). The biogeochemical feedback to the simulated physics could therefore improve the ERSEM skill on the NWE Shelf.

2. Methods

2.1. The physical model: NEMO

The NEMO ocean physics component (OPA) is a finite difference, hydrostatic, primitive equation ocean general circulation model ([25]). The NEMO configuration used in this study is similar to the one used by [45, 46, 31], and identical to the configuration used in [36]: we use the CO6 NEMO version, based on NEMOv3.6, a development of the CO5 configuration explained in detail by [47]. The model has 7 km spatial resolution on the Atlantic Margin Model (AMM7) domain using a terrain-following $z^* - \sigma$ coordinate system with 51 vertical levels ([48]). The lateral boundary conditions for physical variables at the Atlantic boundary were taken from the outputs of the Met Office operational 1/12° North Atlantic model (NATL12, [49]); the Baltic boundary values were derived from a reanalysis produced by the Danish Meteorological Institute for CMEMS. We use annually varying river discharge based on data from [50].

The model was forced at the surface by atmospheric fluxes provided by an hourly and 31km resolution realisation (HRES) of the ERA5 data-set (https://www.ecmwf.int/). In case of the one-way coupled model the ERA5 fluxes provide also the total incoming net shortwave radiation whose visible fraction is attenuated inside the water column based on the Kd for 490nm wavelength supplied by a monthly climatology from an Ocean Color - Climate Change Initiative (OC-CCI) product of European Space Agency (ESA), version 4.1 (https://www.esa-oceancolour- cci.org/). For the two-way coupled model the incoming net short-wave radiation is decomposed into direct and diffuse streams and spectrally resolved, and is provided by the bio-optical module ([31]) that will be described later in the ecosystem model section. The direct and diffuse streams are attenuated throughout the water column by the bio-optical module, and subsequently integrated by NEMO to calculate the heating within each vertical layer.

2.2. The ecosystem model: ERSEM

ERSEM ([28, 29]) is a lower trophic level ecosystem model for marine biogeochemistry, pelagic plankton, and benthic fauna ([51]). The model splits phytoplankton into four functional types largely based on their size ([28]): picophytoplankton, nanophytoplankton, diatoms and dinoflagellates. ERSEM uses variable stoichiometry for the simulated plankton groups ([52, 53]) and each Phytoplankton Functional Type (PFT) biomass is represented in terms

of chlorophyll, carbon, nitrogen and phosphorus, with diatoms also represented by silicon. ERSEM predators are composed of three zooplankton types (mesozooplankton, microzooplankton and heterotrophic nanoflagellates), with organic material being decomposed by one functional type of heterotrophic bacteria ([29]). The ERSEM inorganic component consists of nutrients (nitrate, phosphate, silicate, ammonium and carbon) and dissolved oxygen. The carbonate system is also included in the model ([54]).

We applied in this study the ERSEM configuration from [36], based on a new ERSEM version 20.10, which has an updated benthic component with respect to [29]. The ERSEM parametrization is identical to the one described in [29]. The Atlantic boundary values for nitrate, phosphate, silicate and oxygen were taken from World Ocean Atlas ([55]) and dissolved inorganic carbon from the GLODAP gridded dataset ([56, 57]), while plankton and detritus variables were set to have zero fluxes at the Atlantic boundary.

The irradiance at the ocean surface was calculated using the bio-optical module implemented into the NEMO-FABM-ERSEM AMM7 configuration by [31]. The bio-optical module resolves irradiance spectrally and distinguishes between downwelling direct and diffuse streams. The module is forced by the ERA5 atmospheric inputs (https://www.ecmwf.int/) for total vertically integrated ozone, water vapour, cloud cover, cloud liquid water and sea-level air pressure, as well as by a satellite product for aerosol optical thickness (MODerate resolution Imaging Spectroradiometer, MODIS, https://modis.gsfc.nasa.gov/data/dataprod), and also by data for surface wind speed, air humidity, and air temperature, all provided by the NEMO atmospheric (ERA5) forcing. The attenuation of the irradiance was described in detail by [31], here it is briefly summarized: The module distinguishes between the absorption and backscattering by the sea water and the 4 PFTs based on the model of [58]. The scheme for the underwater irradiance was based on [33], i.e. the irradiance was resolved at 33 wavelengths in the 250 - 3700nm range, and so were the wavelength-dependent absorption and backscattering coefficients for clear water and PFTs. Although we included the impact of backscattering on the light attenuation, similarly to [31], we did not explicitly track the upwelling stream. Besides the clear sea water and PFTs, we included into the light attenuation also the absorption by POM, CDOM and sediment, which was (the same as in [31]) forced by an external product extrapolated from the 443nm data of [59]. The bio-optical module was extensively validated in [31], and was shown to be skilled in its representation of SWR, PAR and the underwater irradiances.

2.3. Observations: assimilated and validation data

2.3.1. Assimilated data

In the physical data assimilation component we have included: a) sea surface temperature data from the GCOM-W1/AMSR-2, NOAA/AVHRR, MetOp/AVHRR, MSG/SEVIRI, Sentinel-3/SLSTR, Suomi-NPP/VIIRS satellite products and in situ SST observations from ships, surface drifters and moorings, distributed over the Global Telecommunication System (GTS) in near-real time, b) temperature and salinity from the EN4 dataset ([60]), which includes in situ profiles from Argo floats, fixed moored arrays, XBTs, CTDs, gliders, marine mammals, and c) temperature and salinity data from a specific Slocum glider Cabot (Unit 345, see [36]) that has been deployed in the central North Sea during 08/05/2018 - 15/08/2018 as a part of the Alternative Framework to Assess Marine Ecosystem Functioning in Shelf Seas (AlterECO) programme (https://altereco.ac.uk/). The satellite SST was bias-corrected following the scheme from [61], using the VIIRS and in situ SST data as the reference.

In the biogeochemical data assimilation we have included total log-chlorophyll derived from the ocean color based satellite product of ESA (version 2.0, [62]) and also log-chlorophyll derived from the fluorescence measurements by the same AlterEco glider Cabot, that was used in the physical data assimilation. The assimilation is performed for log-chlorophyll, rather than chlorophyll, as chlorophyll is widely known to be log-normally distributed ([63]).

The assimilated in situ (EN4, glider) observations were thinned to a resolution of 0.08° (EN4), or up-scaled to the AMM7 grid (glider), with additional temporal averaging applied to the same-day glider observations. The thinning/up-scaling is performed to avoid assimilating many observations at higher resolution than the model can represent. After the thinning/up-scaling there were O(10^5) EN4 and O(10^4) Cabot glider data-points to assimilate throughout the year 2018.

2.3.2. Validation data

The assimilated observations were used for the validation of those experiments in which they were excluded from the assimilation (e.g. chlorophyll data for the physical data assimilative run). However, we excluded the bias-corrected satellite SST from the temperature validation, so that the only assimilated SST data used for validation were a) the high quality SST data from the VIIRS satellite product and from ships, drifters and moorings (we will call this "VIIRS/in situ SST data"), and the SST that was part of b) EN4

and c) Cabot glider data. Besides the assimilated observations, all the experiments were validated with other (non-assimilated) AlterEco glider data for temperature, salinity, chlorophyll, oxygen and the sum of nitrate and nitrite (all the gliders included in the validation are listed in Tab.1). The processing of the physical, chlorophyll and oxygen data was described in [36]. The sum of nitrate and nitrite concentrations (abbreviated as NO_x- = NO_3- + NO_2-) were determined using a Lab-on-Chip (LoC) analyser designed and fabricated at the National Oceanography Centre ([64]), which were implemented by the AlterEco team into Seagliders following a similar protocol as used by [65]. The combined uncertainty (random and systematic errors) of measurements made using these LoC analysers has been calculated as ¡5% (coverage interval $k = 1$) ([66]). The nitrite concentrations were relatively negligible compared to the nitrate concentrations, so the NO_x- data were used to validate model nitrate outputs. All of the used AlterEco gliders operated during 2018 in the central North Sea (for both the glider and the EN4 data locations see Fig.S1 of the Supporting Information (SI)), moving throughout the whole water column. Similar to the assimilated Cabot glider, the remaining glider data were up-scaled onto the model grid (on a daily basis) and after the up-scaling there remained O(10^4) AlterEco glider observations for each variable in 2018.

The EN4 data-set contained subsurface observations that were approximately homogeneously distributed both with depth and in time, with slightly lower number of observations towards the end of the year (November-December 2018). Beyond the assimilated data and the AlterEco data, we used for validation a 1960-2014 monthly climatological dataset for total chlorophyll, oxygen, nitrate, phosphate and silicate concentrations, compiled in the North Sea Biogeochemical Climatology (NSBC) project ([67]). The NSBC dataset covers most of the NWE Shelf and the full range of depths. Finally, we also included validation of surface CO_2 fugacity using 2018 SOCAT (v2019) data (https://www.socat.info/index.php/about/).

2.4. The assimilative system: NEMOVAR

NEMOVAR is a variational (in this study a 3DVar) DA system ([68, 69, 70]) used at the Met Office for operational reanalyses and forecasting on the NWE Shelf. The assimilation of ocean color-derived chlorophyll using NEMOVAR is highly successful in improving the NWE Shelf phytoplankton phenology, PFT community structure (using PFT chlorophyll assimilation), underwater irradiance and to a more limited degree also carbon cycle ([46, 31,

Table 1: The AlterEco gliders and the variables measured by the gliders used for assimilation (6-th column), or validation (7-th column). The table uses the following abbreviations: deployment:"dpl", data assimilation:"DA", temperature:"T", salinity:"S", oxygen concentrations:"O_2", chlorophyll a concentrations:"Chl a" and sum of nitrate and nitrite concentrations:"NO_x-".

Campaign	**platform**	**dpl**	**serial**	**mission period**	**DA**	**validation**
AlterEco 1	Stella	440	unit_436	02/02/2018 - 08/05/2018	none	T,S,O_2,Chl a
AlterEco 1	Cook	441	unit_194	15/11/2017 - 07/02/2018	none	T,S,O_2,Chl a,NO_x-
AlterEco 2	Orca	493	SG510	07/03/2018 - 27/03/2018	none	Chl a,NO_x-
AlterEco 2	Melonhead	496	SG620	07/02/2018 - 02/04/2018	none	Chl a
AlterEco 3	Cabot	454	unit_345	08/05/2018 - 15/08/2018	T,S,Chl a	T,S,O_2,Chl a
AlterEco 3	Orca	455	SG510	16/03/2018 - 24/07/2018	none	Chl a,NO_x-
AlterEco 3	Humpback	497	SG579	09/05/2018 - 25/06/2018	none	Chl a
AlterEco 4	Dolomite	477	unit_305	13/08/2018 - 10/10/2018	none	T,S,Chl a,NO_x-
AlterEco 4	Eltanin	478	SG550	15/08/2018 - 28/09/2018	none	Chl a
Altereco 5	Kelvin	481	unit_444	26/09/2018 - 02/12/2018	none	T,S,Chl a
AlterEco 6	Dolomite	499	unit_305	02/12/2018 - 12/03/2018	none	T,S,O_2,Chl a
AlterEco 6	Coprolite	500	unit_331	02/12/2018 - 12/03/2018	none	T,S,O_2,Chl a

71]). NEMOVAR includes capability to assimilate multi-platform (satellite, in situ) data, which has been established first for physics (e.g. [70, 72]) and subsequently for biogeochemistry ([73]), including validating the multi-platform DA system for the NWE Shelf ([36]).

The NEMOVAR set-up used in this study for the multi-platform physical-biogeochemical assimilation is the same as the one described in detail by [36]. Here we offer only a short summary: The 3DVar version of NEMOVAR uses a First Guess at Appropriate Time (FGAT) to calculate a daily set of increments for the directly updated variables ([70, 72]). In the physical DA application NEMOVAR applies balancing relationships within the assimilation step and delivers a set of increments for temperature, salinity, sea surface height (SSH) and the horizontal velocity components. For the total chlorophyll assimilation NEMOVAR calculates a set of log-chlorophyll increments and then a balancing scheme is used to distribute those increments into the PFT components (chlorophyll, carbon, nitrogen, phosphorus and for diatoms also silicon), all of which are being updated based on the background community structure and stoichiometric ratios (e.g. [46, 31, 36]). After the assimilation step, the model is re-run with the increments applied to the model variables gradually at each model time-step using incremental analysis updates (IAU, [74]).

NEMOVAR uses externally supplied spatio-temporally varying observation and background error variances, with the background error variances typically 1-3 times larger than the observational error variances ([36]). The system combines two horizontal correlation length-scales, one fixed 100km length-scale with another length-scale based on the baroclinic Rossby radius of deformation ([72]). The vertical length-scales follow the scheme from [72], where NEMOVAR calculates directly the set of 3D increments using flow-dependent vertical length-scales (ℓ), which are at the surface equal to half of the MLD, decreasing in the mixed layer to become two-times the vertical model grid spacing at, and beneath the MLD.

2.5. The experiments

In this study we compared the performance of both one-way and two-way coupled versions of the NEMO-FABM-ERSEM model. We also tested the impact of assimilating different types of data (physical-only, biogeochemical-only and physical and biogeochemical jointly) on the skill of both the one-way and two-way coupled models. The various experiments used exactly the same model configuration, apart from the difference in the coupling between physics and biogeochemistry. The experiments all started from the same initial value conditions on the 01/09/2017 to allow a 4 month spin-up time for the final 2018 simulation. The initial values were provided by the 2016-2018 free simulation (using bio-optical module) from the study of [31]. Finally, Tab.2 provides a list of all experiments with their abbreviated names that we will use in the paper.

2.6. Skill metrics

The performance of the different simulations will be evaluated using two skill metrics. The first metric is the model bias (ΔQ_{mo}):

$$\Delta Q_{mo} = \langle Q_m - Q_o \rangle \tag{1}$$

where Q_o are the observations mapped into the model grid and the Q_m are the corresponding model outputs. The second metric is the bias-corrected root mean square difference (BC RMSD, $\Delta_{RD} Q_{mo}$):

$$\Delta_{RD} Q_{mo} = \sqrt{\langle (Q_m - Q_o - \Delta Q_{mo})^2 \rangle}. \tag{2}$$

Table 2: The different experiments compared in this study. The first column shows the abbreviated experiment name, the second column indicates whether the two-way coupling is used and the following columns list the assimilated data. The table uses the following abbreviations: satellite:"sat", Cabot glider:"Cabot", EN4 dataset:"EN4", temperature:"T", sea surface temperature:"SST", salinity:"S", chlorophyll *a*:"Chl *a*".

abbreviation	two-way	SST (sat./in situ)	T & S (EN4)	T & S (Cabot)	Chl *a* (sat.)	Chl *a* (Cabot)
free 1-way	no	no	no	no	no	no
free 2-way	yes	no	no	no	no	no
phys DA 1-way	no	yes	yes	yes	no	no
phys DA 2-way	yes	yes	yes	yes	no	no
chl DA 1-way	no	no	no	no	yes	yes
chl DA 2-way	yes	no	no	no	yes	yes
phys+chl DA 1-way	no	yes	yes	yes	yes	yes
phys+chl DA 2-way	yes	yes	yes	yes	yes	yes

3. Results and Discussion

3.1. The impact of the two-way coupling and assimilation on the simulated physics

The reference one-way coupled model simulates well the seasonal increase of temperature in the surface ocean in late-spring / summer (Fig.2:A, Fig.3). The novel two-way coupling further increased the temperature in the upper 20m by around 1°C (Fig.2:B, Fig.3). This is a relatively major change with respect to the reference run, when compared to the changes introduced to the simulated temperature by the physical data assimilation during the same period of the year (Fig.2:D, for all the assimilative runs see Fig.S2-S3 in the Supporting Information (SI)). The increase in the upper ocean temperature in the two-way coupled model cannot be explained by the enhanced shortwave radiation flux in the water column, since the bio-optical module and the ERA5 short-wave radiation product, which forces the one-way coupled run, have a negligible mutual bias ([31]). Therefore, the temperature increase is likely a consequence of an increased rate of absorption inside the upper oceanic layer. The increased absorption in the two-way coupled run was anticipated since: a) the bio-optical module appears to have higher level of light attenuation near the water surface than the satellite observations used to force the physics in the one-way coupled run (this was observed for 490nm wavelength in Fig.5:A of [31]), b) the "broadband" visible light attenuation in the one-way coupled run was represented by the satellite K_d for 490nm

wavelength, but K_d at 490nm wavelength is clearly an underestimate of the K_d for the 400-700nm waveband (see Fig.5:B of [31]).

The impact of phytoplankton biomass on the simulated temperature can be analysed by comparing the chlorophyll-assimilative run (chl DA 2-way) with its corresponding two-way coupled free run (free 2-way): In the late spring - summer, the assimilation of chlorophyll into the two-way coupled model removes a large amount of phytoplankton biomass from the mixed layer (see Fig.S4:B of SI), increases the light penetration into the water column and heats up a deeper oceanic layer than the free run (Fig.2:B-C). The temperature is then raised in the 20-60m depth range by 0.1-0.2°C in the summer and by less than that in the late spring (see Fig.S5 of SI). The extra heat captured by the two-way coupled model near the ocean surface shallows the MLD (Fig.4:B, Fig.S6 of SI), which is indicative of important changes to mixing of biogeochemical tracers in the upper ocean.

Outside of the late spring - summer, both two-way coupling (Fig.2:B) and chlorophyll assimilation (Fig.2:C) have comparably smaller impact on the simulated oceanic temperature than the physical data assimilation (Fig.2:D, see also Fig.S2-S4 of SI). The impact of physical data assimilation is most important around the winter, when it corrects a negative temperature bias ($\sim$ -0.5°C) of the physical model (Fig.2-3, Fig.S3-S4 of SI). The physical data assimilation influences the simulated temperature more evenly across the water column than the bio-optical module (Fig.2), which is likely a combination of model dynamical response to the temperature increments in the mixed layer and some assimilated sub-surface data (EN4 and Cabot glider). If the reanalysis state is sufficiently stable with respect to the model dynamics, it is known ([46, 31, 36]) that, within NEMOVAR on the NWE Shelf, the assimilated variables in the reanalysis tend to converge to the assimilated data. This is evident in the Fig.5:D, Fig.S3,S7 of SI, comparing the SST of the physical data assimilation runs with the assimilated satellite SST observations.

We evaluated (Fig.6 and Fig.7) the skill of both the two-way coupled model and the different assimilative experiments to represent temperature and salinity on the NWE Shelf. Fig.6 compares the two-way coupled free and chlorophyll-assimilative runs with the temperature and salinity measured by the Cabot glider mission in the central North Sea during late spring - summer of 2018 (for more details about the mission see [36], Fig.S1 of SI and Tab.1). Glider-observed temperature is warmer in the upper 30-40m of the water column than the temperature simulated by the one-way coupled model, whereas

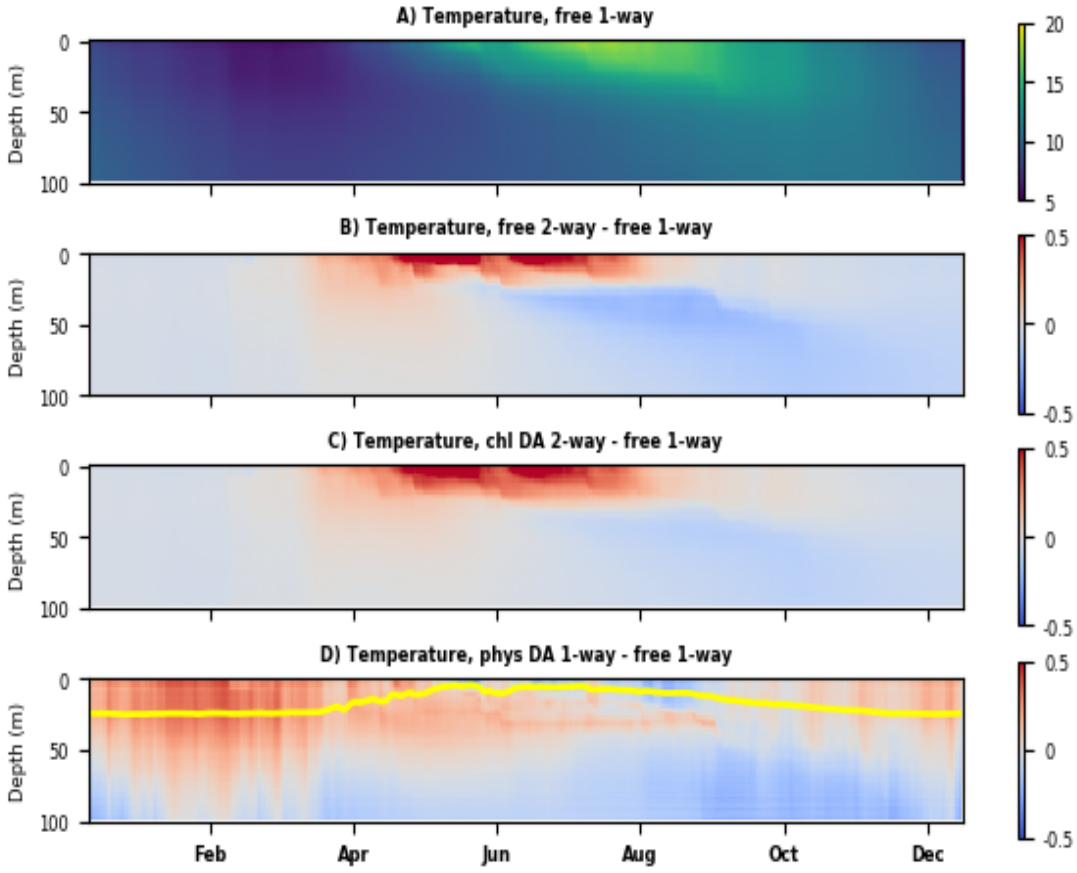

Figure 2: Panel A shows Hovmöller diagram (time on the x-axis vs depth on the y-axis) for the temperature (°C) of the one-way coupled free run, where the values for each day and depth represent the horizontal spatial averages throughout the NWE Shelf (bathymetry < 200m). Panels B-D show the same Hovmöller diagrams as panel A, but for the temperature differences between the two-way coupled, or assimilative runs and the reference, free one-way coupled model run from the panel A (for the abbreviations used in the titles see Tab.2). In particular, panels B-D compare the impact of two-way coupling on the simulated temperature (panel B), joint impact of chlorophyll-assimilation and two-way coupling on the simulated temperature (panel C) and the impact of physical data assimilation on the simulated temperature (panel D). The yellow line in the panel D shows the MLD of the physical data assimilative run to indicate the vertical scale of impact of the SST assimilation.

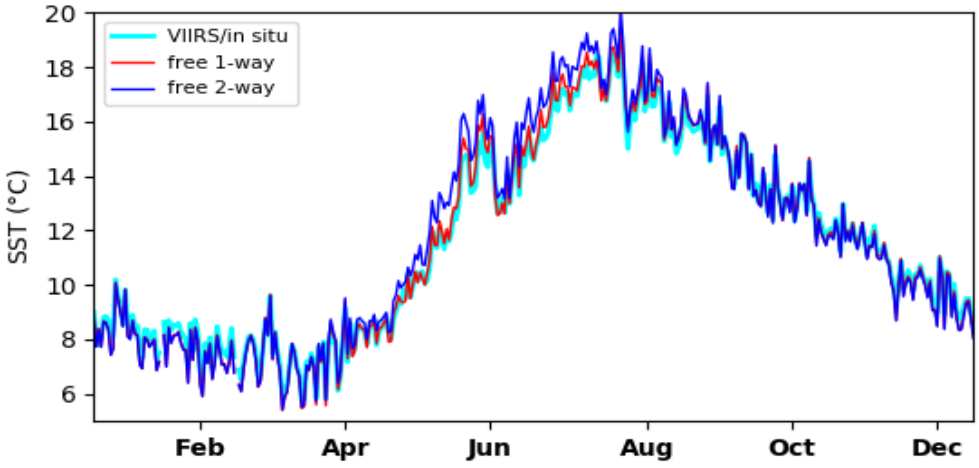

Figure 3: The 2018 time-series of SST averaged throughout the NWE Shelf compared between the one-way and two-way coupled free simulations, and the VIIRS satellite/in situ data. To consistently compare the model simulations with the observed SST, the model outputs were masked wherever there were missing observations. The missing satellite observations are due to the movements of clouds and atmospheric disturbances and the missing values are responsible for the small time-scale fluctuations in the different curves shown in the plot.

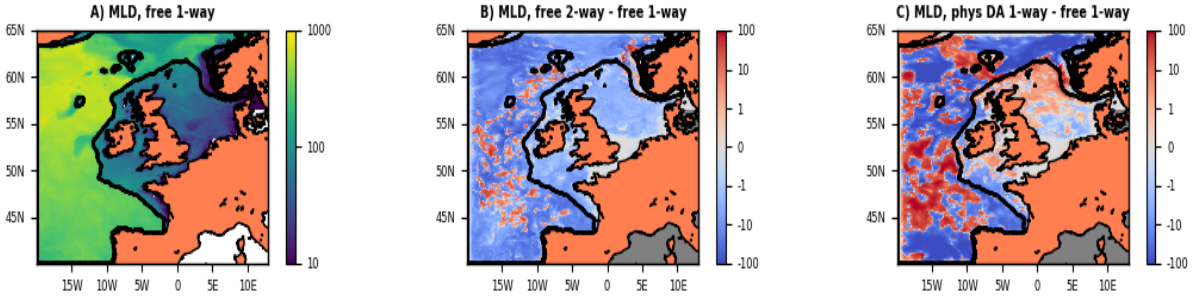

Figure 4: Panel A shows the mixed layer depth (MLD, in m) of the one-way coupled reference free run. The MLD values are averaged for the spring bloom period between March-May 2018. Panels B-C show the relative changes in MLD carried by the two-way coupled free run (panel B) and physical data assimilation into the one-way coupled model (panel C). Both panels B,C show the difference (in m) between the MLD of the two-way coupled, or physical data assimilative run and the one-way coupled model free run (panel A). The blue color in panels B-C (negative values) indicates shallowing of MLD, whilst the red color (positive values) indicates deepening of MLD. The black line shows the boundary of the continental shelf (bathymetry $<$ 200m).

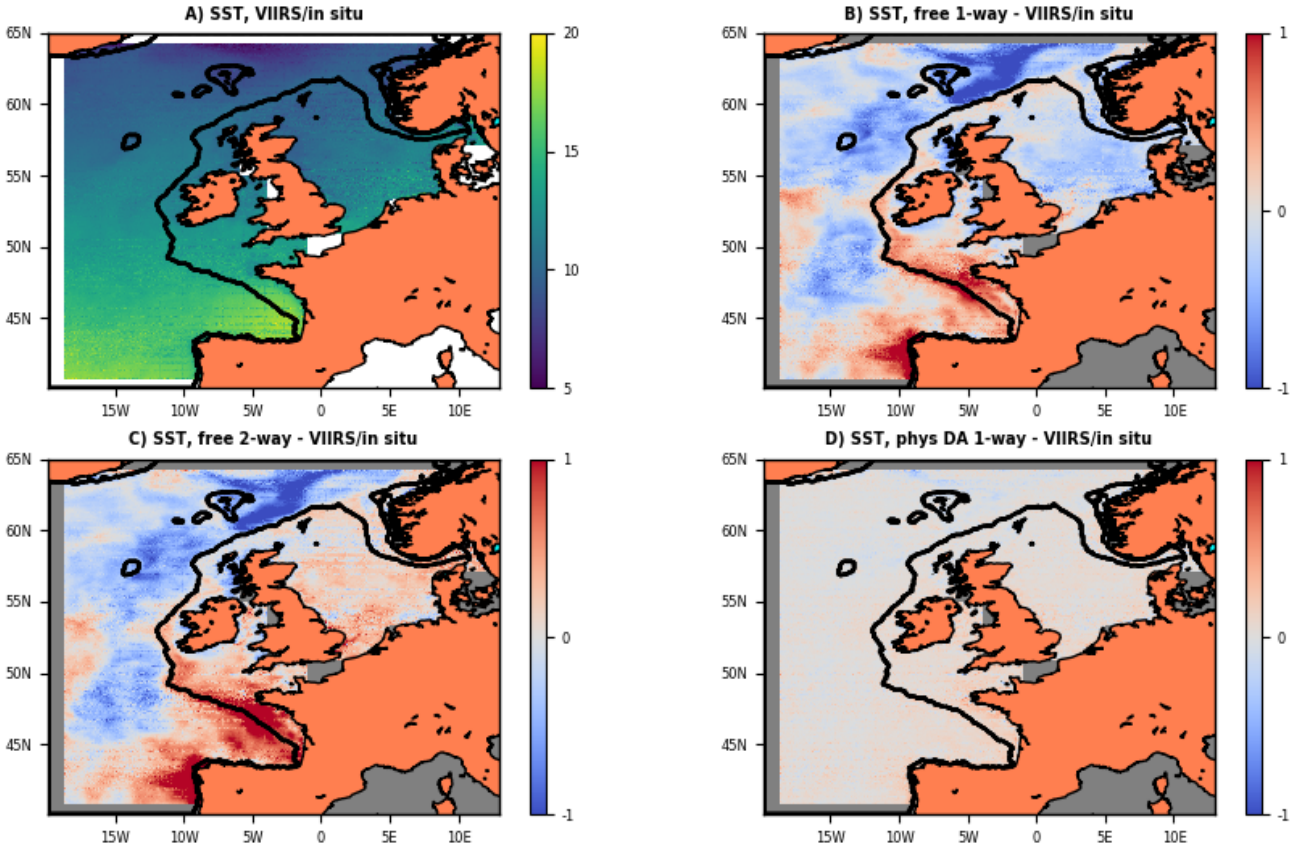

Figure 5: The assimilated 2018 median satellite data for SST (panel A, in °C) and the corresponding model to VIIRS/in situ SST differences (panels B-D, in °C) for one-way coupled model free run (panel B), two-way coupled model free run (panel C) and physical data assimilation into the one-way coupled free run (panel D). The masked values indicate the regions where there was no assimilation of VIIRS/in situ data into the model.

the opposite is true beneath 40m depth (Fig.6:A). This means the observed thermocline represents a larger gradient in temperature than the simulated thermocline. The bio-optical module substantially (by $> 1°C$) heats up the upper 20-30m layer, increasing the vertical temperature gradient (Fig.6:C), however the near-surface temperature of the two-way coupled run rises well above the levels observed by the glider (Fig.6:D). The thermocline of the two-way coupled model free run appears to be located above the glider thermocline (e.g. Fig.6:D) and the impact of the two-way coupling on the model skill in representing glider temperature is somewhat mixed (it improves bias, but degrades BC RMSD, Fig.7:A). The skill validation presented in Fig.7 shows similarly mixed results: the summer temperature bias is improved across the EN4 and AlterEco glider data, but degraded relative to the VIIRS/in situ data (see also Fig.3), with the BC RMSD consistently degraded across the different validation data. The Fig.7:A indicates that the two-way coupling produces better results for sub-surface summer temperature, than for SST (VIIRS/in situ data). The two-way coupling has a similarly mixed impact on the free run skill to represent summer salinity (Fig.7:C), and both small ($< 0.05°C$) and mixed impact on winter temperature and salinity (Fig.7:B,D, for temperature see also Fig.2-3). However, it should be noted that chlorophyll assimilation into the two-way coupled model slightly improves the skill of the free run in representing temperature and salinity across most of the data and throughout the whole year 2018 (Fig.7). Finally, the comparison with the non-assimilated temperature validation data clearly demonstrates that the physical data assimilation improves the model skill in temperature both in summer and winter half-year (Fig.7:A-B) and also the model skill in salinity in the winter half-year (Fig.7:D).

3.2. The impact of the two-way coupling and assimilation on biogeochemistry

As the days in spring become longer, the layer that is effectively lit by the sunlight expands into the water column, whilst the effective mixing depth shrinks. It is often assumed, that the effective mixing depth reaching a critical threshold marks the onset of the spring bloom (Fig.1). This process might be misrepresented by the one-way coupled reference free simulation, which could be why the model shows on the NWE Shelf late (by ~ 1 month) and intense blooms (Fig.8, see also [31, 36]). The effective mixing depth has often been interpreted as the seasonal MLD (this is the frequent understanding of the critical depth hypothesis of [75]), but it is assumed that on the NWE Shelf the onset of the bloom might be better described by the critical turbulence

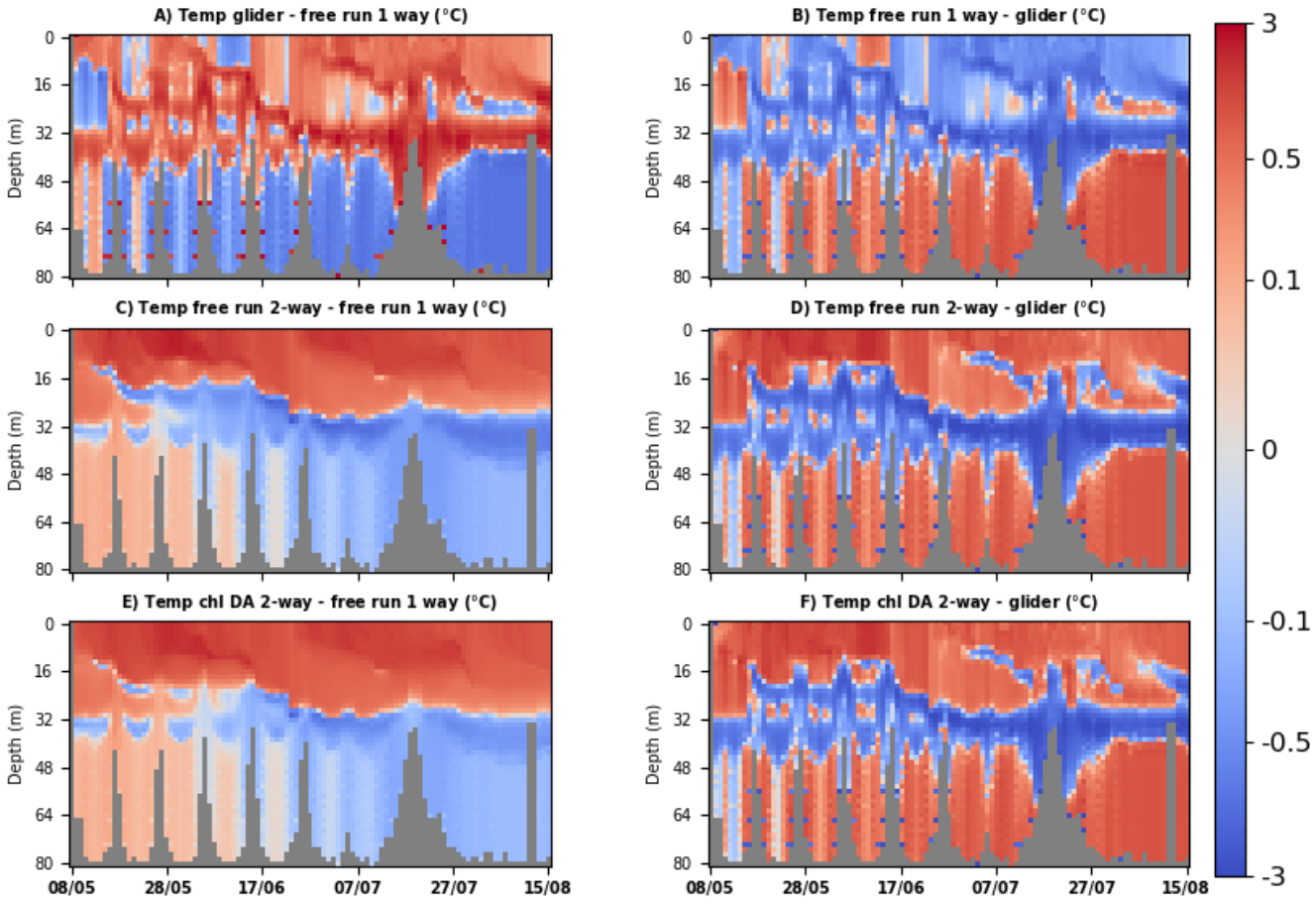

Figure 6: Hovmöller diagram for temperature (°C) along the trajectory covered by the Cabot glider in the central North Sea during an early May to mid-August 2018 mission. The right-hand panels (B,D,F) show the temperature differences between the free one-way coupled run (panel B), free two-way coupled run (panel D), the chlorophyll assimilation into the two-way coupled model (panel F) and the Cabot glider observations (model minus glider). The left hand panels (A,C,E) show the differences between the observations, or model simulations and the reference, free one-way coupled model run. The purpose of the left-hand panels is to show the desired changes to the one-way coupled model (panel A) and how these changes are realized by the biogeochemical feedback in the free run (panel C) and in the chlorophyll-assimilative run (panel E). The main advantage of those left-hand (A,C,E) panels is that they allow relatively easy interpretation of the dynamical changes introduced to the reference run by the biogeochemical feedback to physics and/or data assimilation.

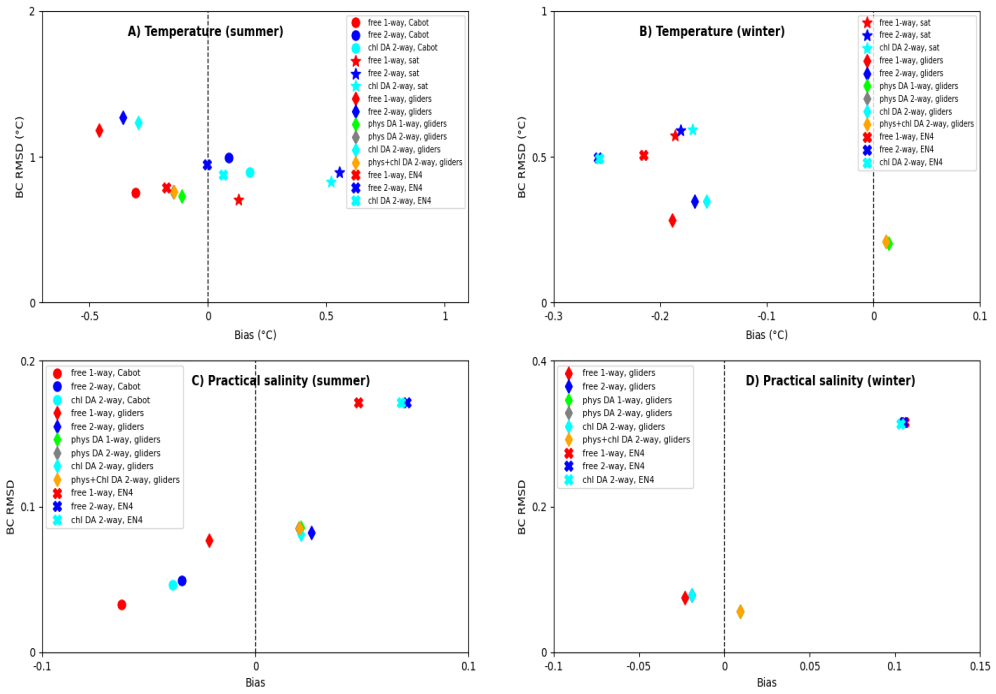

Figure 7: Skill of the different model simulations to represent temperature (°C, panels A-B) and practical salinity (panels C-D). The skill is measured by bias (x-axis, Eq.1) and BC RMSD (y-axis, Eq.2). The skill is evaluated for two half-year periods of 2018, the "summer" (panels A,C) defined as May-October and the "winter" (panels B,D) defined as November-April (data averaged through January-April 2018 and November-December 2018). The different simulations are represented by different colors: free run of the one-way coupled model (red), free run of the two-way coupled model (blue), assimilation of chlorophyll into the two-way coupled model (cyan), physical data assimilation into the one-way coupled model (lime), physical data assimilation into the two-way coupled model (grey) and joint physical data-chlorophyll assimilation into the two-way coupled model (orange). The different markers show comparison with different data-sets: the star stands for the VIIRS/in situ SST, the circle for the Cabot glider observations, the diamond for the remaining available glider observations (the 2018 AlterEco mission without Cabot) and the cross for the EN4 data-set. The data (SST, Cabot, EN4) which were assimilated in some of the simulations were used to validate only the simulations that avoided their assimilation.

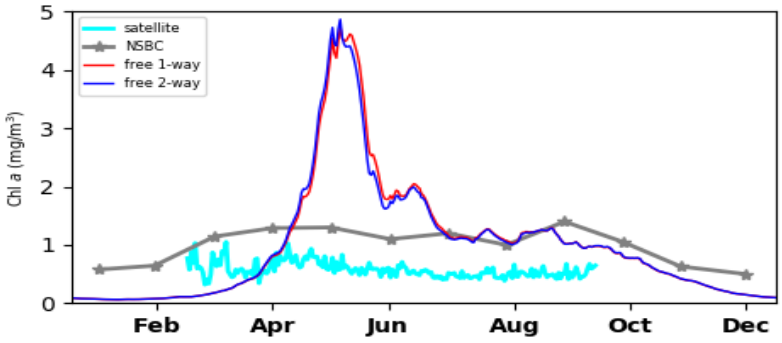

Figure 8: The 2018 time-series of surface chlorophyll a concentrations (mg/m^3) averaged throughout the NWE Shelf compared between the one-way and two-way coupled free simulations, the satellite data, as well as with the NSBC climatological data-set. The satellite data were considered only in the March-September period as the data outside this period are scarce and limited only to the southern part of the NWE domain. The small time-scale fluctuations in the satellite data are due to the missing values caused by the movement of clouds and atmospheric disturbances.

hypothesis ([40]). In the critical turbulence hypothesis the bloom starts when the turbulent mixing in the upper ocean drops beneath a critical level, whilst the effective rate of turbulent mixing is largely decoupled from the seasonal MLD ([40, 41, 42]).

The implementation of the bio-optical module was shown to shallow the MLD (Fig.4), but it can also reduce convection within the mixed layer and the turbulent mixing. The starting hypothesis of this work was that the extra heat captured in the upper oceanic layer could trigger an earlier bloom and improve the ERSEM skill. Fig.8, Fig.9:B and Fig.10:C-D show that the changes to the simulated physics introduced through the two-way coupled model indeed trigger an earlier phytoplankton bloom, but the difference in the bloom timing is only on the scale of several days, rather than weeks. However, the shift to the bloom timing has an impact on many subsequent features, such as the deep chlorophyll maxima (e.g. [36]), so the changes to the bloom onset can gradually propagate to the subsurface chlorophyll (Fig.9:C). The model skill to simulate chlorophyll is improved by the two-way coupling quite notably in the central North Sea and the period covered by the Cabot glider (Fig.11:A), however comparisons with other data spread throughout the year 2018 (satellite ocean color, remaining AlterEco gliders and the NSBC climatology) show only small improvement (Fig.11:A). The

modest improvement to the timing of the (delayed) spring bloom through the changed mixing is certainly a disappointment, and we suspect that to introduce a larger correction to the timing of the bloom it would be necessary to either improve the physical model mixing scheme, or to improve some key ERSEM parameters and processes, such as P-I curves, the maximum chlorophyll-to-carbon ratios, zooplankton grazing and representation of plankton mixotrophy ([29]).

Although the (modest) improvements to the simulated chlorophyll by the two-way coupled model originate from its changes to the simulated physics (i.e. vertical mixing), the physical data assimilation, which substantially improves the simulated physics (Fig.7) does not improve (even slightly degrades) the model skill in chlorophyll (Fig.11:A). This is likely because the physical data assimilation is for large part the assimilation of SST. The improvement in the ecosystem model skill depends mostly on the vertical mixing and limited changes to vertical mixing are expected by assimilating SST. Assimilated subsurface temperature and salinity data are quite sparse, and have only a limited impact on the modelled biogeochemistry. In the case of the Cabot glider "case-study" presented in Fig.10 (for a more complete view see Fig.S8 of SI), the glider temperature and salinity assimilation did not improve the simulated chlorophyll at the glider locations (Fig.11:A) mostly because the impact of physics on biogeochemistry needs some spin-up time. In fact in the last part of the glider mission period (late July-August in Fig.10:E) the physical assimilation has some potential to improve the chlorophyll concentrations, as was demonstrated by the assimilation of the same Cabot glider data in Fig.6E of [36]. Finally, the chlorophyll assimilation dominates over both physical assimilation and two-way coupling in its impact on the simulated chlorophyll concentrations across the whole water column and the whole simulation year (Fig.9:D and Fig.S9 of SI). Since the chlorophyll assimilation is almost entirely based on the satellite ocean color, chlorophyll beneath the mixed layer is updated through the model dynamical response to the assimilation (e.g. vertical mixing). Similarly to temperature, the chlorophyll reanalyses look very similar to the assimilated data (Fig.12:B-C, Fig.S5 and Fig.S10 of SI) and also validate much better than the free runs relative to the non-assimilated AlterEco glider data (Fig.11:A).

We validated the model simulation of additional biogeochemical variables with available observational data: oxygen, nitrate, phosphate, silicate and CO_2 fugacity. The oxygen concentrations are mostly driven by the primary productivity, respiration and outgassing, which largely depends on the sea

temperature. The two-way coupled model improves the model skill in representing Cabot oxygen (Fig.11:B), which is likely triggered by the fact that the same simulation improves both Cabot chlorophyll (Fig.11:A) and the temperature bias (Fig.7:A). Equivalently, model skill in representing Cabot glider oxygen can be improved by assimilating physical data into the model (phys DA 1-way), and it is to some degree also improved by assimilating chlorophyll (chl DA 1-way, chl DA 2-way), with the best performance achieved when both the physical data and chlorophyll are assimilated into the model (Fig.11:B). However, the Cabot glider study is specific, since the glider mission took place in the period of the largest discrepancy in the simulated and observed productivity (Fig.8) and the oxygen concentrations were measured by the same glider that provided temperature, salinity and chlorophyll data for assimilation. For the remaining non-assimilated AlterEco gliders the impact of two-way coupling and assimilation on simulated oxygen is less clear (Fig.11:B), i.e. even though AlterEco chlorophyll is improved by the chlorophyll-only assimilative runs (Fig.11:A) they mostly degrade simulated oxygen (Fig.11:B). This is likely due to the complex relationship between phytoplankton chlorophyll and oxygen (see [36]), which includes respiration of oxygen by the higher trophic-level species (in ERSEM it is zooplankton and heterotrophic bacteria). However, improved representation of temperature consistently improves model oxygen bias across all the used data (Fig.11:A), which indicates that an important part of oxygen bias is due to model biases in temperature and not due to errors in the simulated biogeochemistry.

Besides oxygen, we looked at the model skill in how it represents the surface CO_2 fugacity, which is influenced by the model skill in simulating primary productivity and sea temperature (gas solubility). Fig.11:C shows that CO_2 fugacity is substantially improved by all the runs that included chlorophyll assimilation, which indicates that the assimilation of chlorophyll improved the phytoplankton carbon biomass and therefore the simulated carbon cycle (see also [46]). The physical data-only assimilative runs, and the two-way coupled free run, had more limited impact on the model skill to represent surface CO_2 fugacity, but they sometimes reduced the model bias in CO_2 fugacity. Both the two-way coupling and the physical assimilation, have a relatively small impact on the nitrate and phosphate concentrations (Fig.11:D-E), however the changed phytoplankton biomass through the chlorophyll assimilation lowers the nitrate and phosphate concentrations at the NSBC data-set locations. This has a positive impact on the nitrate bias and a negative impact on the phosphate bias (Fig.11:D-E). Silicate is

impacted more by the physical data assimilation than nitrate and phosphate, but it is mostly degraded by all the assimilative runs (Fig.11:F).

4. Summary

In this work we used a recently developed bio-optical module to improve the representation of oceanic heat fluxes and to introduce a biogeochemical feedback to the physical marine model (we call the model with such feedback "a two-way coupled model"). We have estimated the scale of the biogeochemical impact on the simulated physics and we have shown that in the upper oceanic layer, in the late spring - summer period, the feedback is comparable to the physical data assimilation in its impact on the simulated temperature. The bio-optical module increases the heat captured in the upper part of the water column, steepens the vertical temperature gradient and shallows the mixed layer depth. We have shown that the changes introduced by the bio-optical module into the physical marine model have a mixed impact on the physical model skill. The skill is however (slightly) improved by the chlorophyll assimilation into the two-way coupled model and substantially improved by the physical data assimilation.

The increased stratification of the water column and the shallowed mixed layer depth have a modest positive impact on the timing of the late bloom displayed by the biogeochemical model. The shift in the timing of the bloom in the two-way coupled model improves the model skill in representing chlorophyll. We conclude that, for a more substantial improvement of the timing of the bloom, it will be necessary to either improve the physical model mixing scheme, or to improve the process description, or parametrization of the biogeochemical model. We have expanded our analysis to include other biogeochemical tracers, and we have found that the two-way coupled model and the physical data assimilation may sometimes help improve the agreement of simulated oxygen concentrations and CO_2 fugacity with observations, both due to improved simulation of the sea water temperature (saturation levels) and productivity.

This study provides important evidence to support the inclusion of two-way coupling into future operational models of the NWE Shelf. Furthermore, the physical-biogeochemical assimilative runs on the NWE Shelf, including this work, are typically only weakly coupled (for one recent exception see [76]), in the sense that the physical and the biogeochemical variables are updated independently and interact only through the model dynamics. The

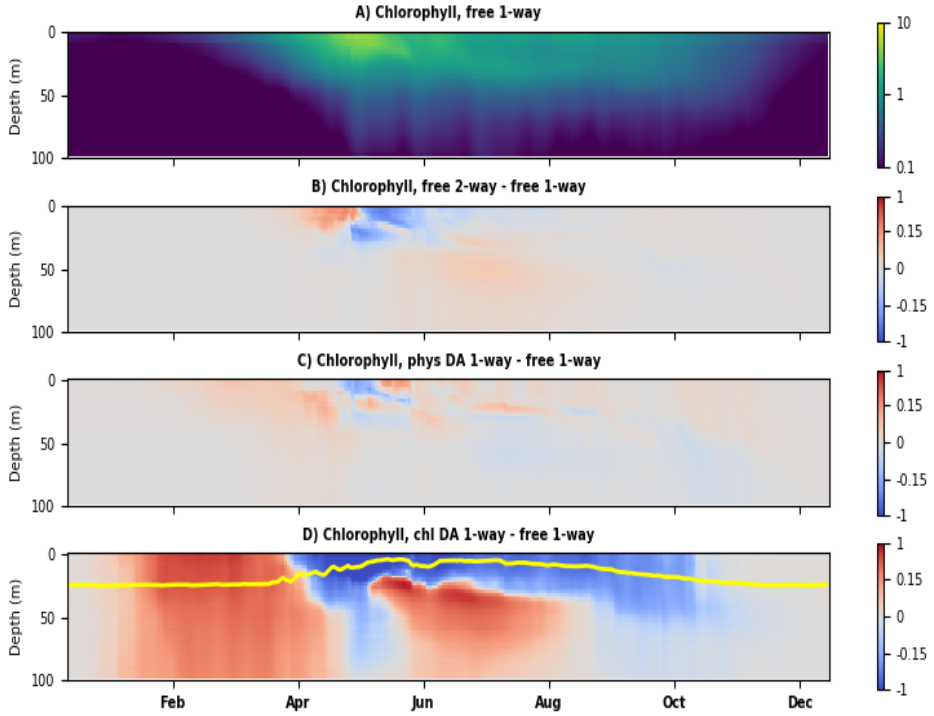

Figure 9: Impact of two-way coupling and assimilation on the simulated chlorophyll concentrations (mg/m^3). Panel A shows Hovmöller diagram (time on the x-axis vs depth on the y-axis) for the one-way coupled model free run, where the values for each day and depth represent the horizontal spatial averages throughout the NWE Shelf (bathymetry < 200m). Panels B-D show the same Hovmöller diagrams, but for the difference between the specific simulation and the reference, free one-way coupled run. The purpose of the panels B-D is to provide an understanding of how the two-way coupling (panel B), the biogeochemical feedback (panel C) and the chlorophyll-assimilation (panel D) influence the chlorophyll concentrations of the reference free one-way coupled run. The yellow line in the panel D shows the mixed layer depth, providing the boundary of the region in which the ocean color assimilation directly updates the simulated chlorophyll.

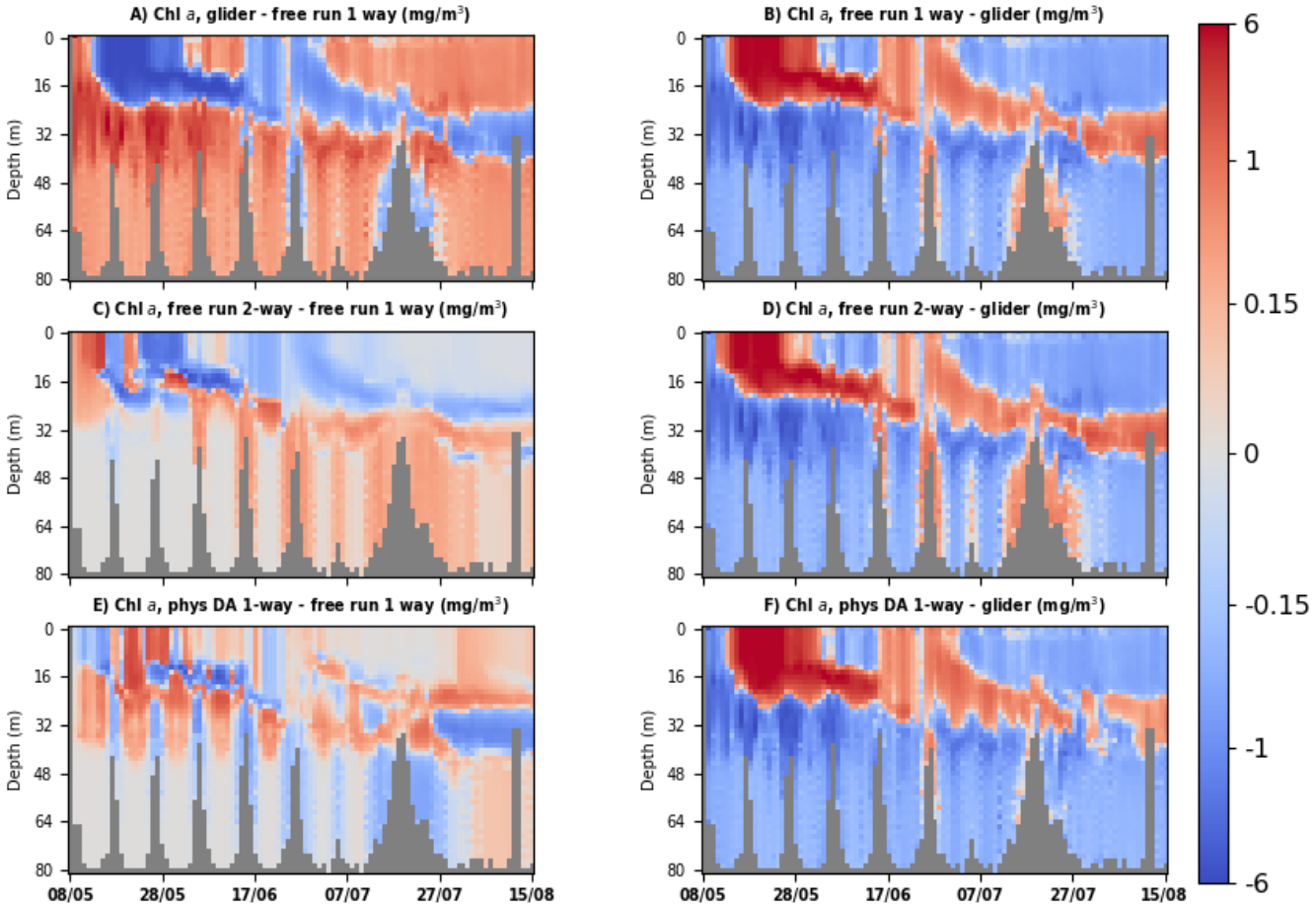

Figure 10: Hovmöller diagram for chlorophyll concentrations (mg/m^3) along the Cabot glider trajectory in the central North Sea during an early May to mid-August 2018 mission. The right-hand panels (B,D,F) show the chlorophyll differences between the free one-way coupled model run (panel B), free two-way coupled model run (panel D), the physical data assimilation into the one-way coupled model (panel F), and the Cabot glider observations (model minus glider). The left hand panels (A,C,E) show the differences between the observations, or model simulations and the reference, free one-way coupled model run. The purpose of the left-hand panels is to show the desired changes to the one-way coupled model (panel A) and how these changes are realized by the biogeochemical feedback in the free run (panel C) and in the physical data-assimilative run (panel E). The main advantage of those left-hand panels is that they allow relatively easy interpretation of the dynamical changes introduced to the reference run by the biogeochemical feedback to physics and/or data assimilation.

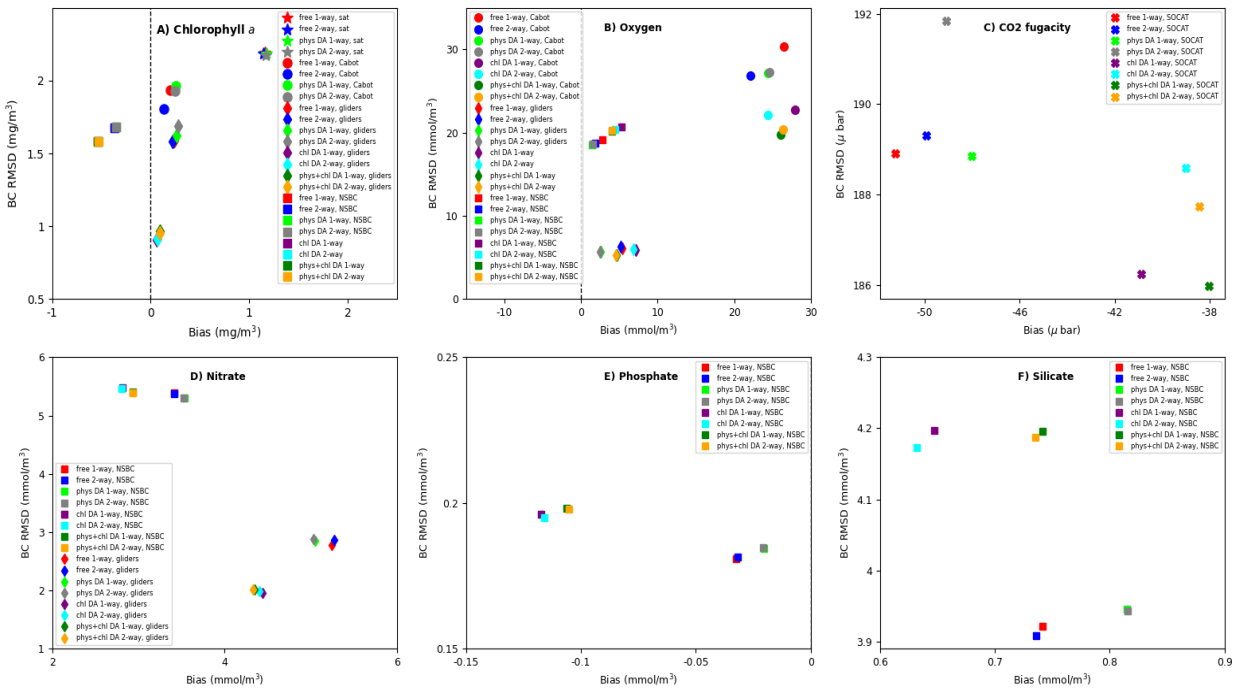

Figure 11: Skill of the different model simulations to represent chlorophyll a (mg/m^3, panel A), oxygen (mmol/m^3, panel B), CO_2 fugacity (μ bar, panel C), nitrate (mmol/m^3, panel D), phosphate (mmol/m^3, panel E) and silicate (mmol/m^3, panel F) concentrations. The skill is measured by bias (x-axis, Eq.1) and BC RMSD (y-axis, Eq.2). The skill is evaluated for the full year 2018. The different simulations are represented by different colors: free run of the one-way coupled model (red), free run of the two-way coupled model (blue), assimilation of chlorophyll into the one-way coupled model (purple), assimilation of chlorophyll into the two-way coupled model (cyan), physical data assimilation into the one-way coupled model (lime), physical data assimilation into the two-way coupled model (grey), joint physical data-chlorophyll assimilation into the one-way coupled model (green) and joint physical data-chlorophyll assimilation into the two-way coupled model (orange). The different markers show comparison with different data-sets: the star stands for the satellite ocean color data, the circle for the Cabot glider observations, the diamond for the remaining available glider observations (the 2018 AlterEco mission without Cabot), the cross for the SOCAT data and the square for the NSBC climatological data-set.

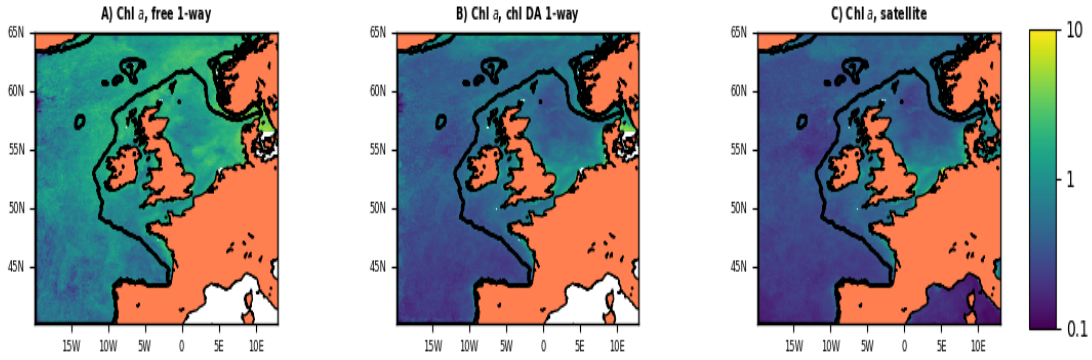

Figure 12: The 2018 mean surface chlorophyll concentrations (in mg/m^3). The different panels compare: the one-way coupled model free run (panel A), the chlorophyll assimilation into the one-way coupled model free run (panel B), and the assimilated satellite ocean color observations (panel C). In the annual averaging we masked the model outputs wherever the satellite data were missing. The black line shows the continental shelf boundary (bathymetry $<$ 200m).

interaction between physics and biogeochemistry via the coupled model dynamics has been strengthened through the two-way coupling, but it would be much more efficient if the assimilative updates to the physics and biogeochemistry interacted directly through their cross-covariances, or a balancing component within a data assimilation system. Such scheme is called "strongly coupled", and would provide the physical assimilation with both faster and greater impact on the biogeochemical model skill, and vice versa. Future work will use the two-way coupled model and expand the data assimilation scheme to include such strong coupling into our operational system.

Acknowledgments

This work was supported by a Natural Environment Research Council (NERC) funded project of the Marine Integrated Autonomous Observing Systems (MIAOS) programme: Combining Autonomous observations and Models for Predicting and Understanding Shelf seas (CAMPUS). It also benefitted from another NERC funded project Alternative Framework to Assess Marine Ecosystem Functioning in Shelf Seas (AlterECO, http://projects.noc.ac.uk/altereco/), grant no. NE/P013899/1. The work also benefited from the Copernicus Marine Environment Monitoring Service (CMEMS) funded projects OPTIcal data Modelling and Assimilation (OPTIMA) and NOWMAPS.

Furthermore, this work was also partially funded by the SEAMLESS project, which received funding from the European Union's Horizon 2020 research and innovation programme under grant agreement No 101004032. We would like to thank Dawn Ashby for drawing the schematic Fig.1. The ocean color data were provided by the European Space Agency Climate Initiative "Ocean Color" (https://esa-oceancolour-cci.org/). The glider data used in the study (doi:10.5285/b57d215e-065f-7f81-e053-6c86abc01a82 and doi:10.5285/b58e83f0-d8f3-4a83-e053-6c86abc0bbb5) are publicly available on https://www.bodc.ac.uk/-data/published_data_library/catalogue/. The model was forced by the atmospheric ERA5 product of The European Centre for Medium-Range Weather Forecasts (ECMWF, https://www.ecmwf.int/). The river forcing data used by the model were prepared by Sonja van Leeuwen and Helen Powley as part of UK Shelf Seas Biogeochemistry programme (contract no. NE/K001876/1) of the NERC and the Department for Environment Food and Rural Affairs (DEFRA). We acknowledge use of the MONSooN system, a collaborative facility supplied under the Joint Weather and Climate Research Programme, a strategic partnership between the Met Office and the NERC. The different outputs for the free run simulations and reanalyses are stored on the MONSooN storage facility MASS and can be obtained upon request.

References

[1] M. Gehlen, R. Barciela, L. Bertino, P. Brasseur, M. Butenschön, F. Chai, A. Crise, Y. Drillet, D. Ford, D. Lavoie, et al., Building the capacity for forecasting marine biogeochemistry and ecosystems: recent advances and future developments, Journal of Operational Oceanography 8 (sup1) (2015) s168–s187.

[2] D. Ford, S. Kay, R. McEwan, I. Totterdell, M. Gehlen, Marine biogeochemical modelling and data assimilation for operational forecasting, reanalysis, and climate research, New Frontiers in Operational Oceanography (2018) 625–652.

[3] C. Heinze, M. Gehlen, Modeling ocean biogeochemical processes and the resulting tracer distributions, in: International Geophysics, Vol. 103, Elsevier, 2013, pp. 667–694.

[4] U. Riebesell, A. Körtzinger, A. Oschlies, Sensitivities of marine carbon

fluxes to ocean change, Proceedings of the National Academy of Sciences 106 (49) (2009) 20602–20609.

[5] Z. Jin, T. P. Charlock, W. L. Smith Jr, K. Rutledge, A parameterization of ocean surface albedo, Geophysical research letters 31 (22) (2004).

[6] A. Morel, Optical modeling of the upper ocean in relation to its biogenous matter content (case i waters), Journal of geophysical research: oceans 93 (C9) (1988) 10749–10768.

[7] J.-y. Simonot, E. Dollinger, H. Le Treut, Thermodynamic-biological-optical coupling in the oceanic mixed layer, Journal of Geophysical Research: Oceans 93 (C7) (1988) 8193–8202.

[8] S. Sathyendranath, A. D. Gouveia, S. R. Shetye, P. Ravindran, T. Platt, Biological control of surface temperature in the arabian sea, Nature 349 (6304) (1991) 54.

[9] A. M. Edwards, D. G. Wright, T. Platt, Biological heating effect of a band of phytoplankton, Journal of Marine Systems 49 (1-4) (2004) 89–103.

[10] M. Manizza, C. Le Quéré, A. J. Watson, E. T. Buitenhuis, Bio-optical feedbacks among phytoplankton, upper ocean physics and sea-ice in a global model, Geophysical Research Letters 32 (5) (2005).

[11] C. Sweeney, A. Gnanadesikan, S. M. Griffies, M. J. Harrison, A. J. Rosati, B. L. Samuels, Impacts of shortwave penetration depth on large-scale ocean circulation and heat transport, Journal of Physical Oceanography 35 (6) (2005) 1103–1119.

[12] M. Lengaigne, C. Menkes, O. Aumont, T. Gorgues, L. Bopp, J.-M. André, G. Madec, Influence of the oceanic biology on the tropical pacific climate in a coupled general circulation model, Climate Dynamics 28 (5) (2007) 503–516.

[13] L. Zhai, C. Tang, T. Platt, S. Sathyendranath, Ocean response to attenuation of visible light by phytoplankton in the gulf of st. lawrence, Journal of Marine Systems 88 (2) (2011) 285–297.

[14] A. Turner, M. Joshi, E. Robertson, S. Woolnough, The effect of arabian sea optical properties on sst biases and the south asian summer monsoon in a coupled gcm, Climate dynamics 39 (3-4) (2012) 811–826.

[15] J. E. Lovelock, R. Maggs, R. Rasmussen, Atmospheric dimethyl sulphide and the natural sulphur cycle, Nature 237 (5356) (1972) 452–453.

[16] R. J. Charlson, J. E. Lovelock, M. O. Andreae, S. G. Warren, Oceanic phytoplankton, atmospheric sulphur, cloud albedo and climate, Nature 326 (6114) (1987) 655–661.

[17] K. D. Six, S. Kloster, T. Ilyina, S. D. Archer, K. Zhang, E. Maier-Reimer, Global warming amplified by reduced sulphur fluxes as a result of ocean acidification, Nature Climate Change 3 (11) (2013) 975–978.

[18] J. Schwinger, J. Tjiputra, N. Goris, K. D. Six, A. Kirkevåg, Ø. Seland, C. Heinze, T. Ilyina, Amplification of global warming through ph dependence of dms production simulated with a fully coupled earth system model, Biogeosciences 14 (15) (2017) 3633.

[19] T. W. Wilson, L. A. Ladino, P. A. Alpert, M. N. Breckels, I. M. Brooks, J. Browse, S. M. Burrows, K. S. Carslaw, J. A. Huffman, C. Judd, et al., A marine biogenic source of atmospheric ice-nucleating particles, Nature 525 (7568) (2015) 234–238.

[20] J. Lovelock, Gaia: A new look at life on earth, Oxford Paperbacks, 1979.

[21] J. Lovelock, The ages of Gaia: A biography of our living earth, Oxford University Press, USA, 2000.

[22] A. Borges, L.-S. Schiettecatte, G. Abril, B. Delille, F. Gazeau, Carbon dioxide in european coastal waters, Estuarine, Coastal and Shelf Science 70 (3) (2006) 375–387.

[23] R. A. Jahnke, Global synthesis, in: Carbon and nutrient fluxes in continental margins, Springer, 2010, pp. 597–615.

[24] O. Legge, M. Johnson, N. Hicks, T. Jickells, M. Diesing, J. Aldridge, J. Andrews, Y. Artioli, D. C. Bakker, M. T. Burrows, et al., Carbon on the northwest european shelf: Contemporary budget and future influences, Frontiers in Marine Science 7 (2020) 143.

[25] G. Madec, et al., Nemo ocean engine (2015).

[26] J. Bruggeman, K. Bolding, A general framework for aquatic biogeochemical models, Environmental modelling & software 61 (2014) 249–265.

[27] J. Bruggeman, K. Bolding, Framework for aquatic biogeochemical models (2020). doi:http://doi.org/10.5281/zenodo.3817997.

[28] J. Baretta, W. Ebenhöh, P. Ruardij, The european regional seas ecosystem model, a complex marine ecosystem model, Netherlands Journal of Sea Research 33 (3-4) (1995) 233–246.

[29] M. Butenschön, J. Clark, J. N. Aldridge, J. I. Allen, Y. Artioli, J. Blackford, J. Bruggeman, P. Cazenave, S. Ciavatta, S. Kay, et al., Ersem 15.06: a generic model for marine biogeochemistry and the ecosystem dynamics of the lower trophic levels, Geoscientific Model Development 9 (4) (2016) 1293–1339.

[30] P. M. L. Marine Systems Modelling Group, European regional seas ecosystem model (2020). doi:http://doi.org/10.5281/zenodo.3817997.

[31] J. Skákala, J. Bruggeman, R. J. Brewin, D. A. Ford, S. Ciavatta, Improved representation of underwater light field and its impact on ecosystem dynamics: a study in the north sea, Journal of Geophysical Research: Oceans (2020) e2020JC016122.

[32] W. W. Gregg, N. W. Casey, Skill assessment of a spectral ocean–atmosphere radiative model, Journal of Marine Systems 76 (1-2) (2009) 49–63.

[33] W. W. Gregg, C. S. Rousseaux, Directional and spectral irradiance in ocean models: effects on simulated global phytoplankton, nutrients, and primary production, Frontiers in Marine Science 3 (2016) 240.

[34] W. W. Gregg, C. S. Rousseaux, Simulating pace global ocean radiances, Frontiers in Marine Science 4 (2017) 60.

[35] J. Bruggeman, J. Skákala, J. Lawrence, D. Ford, R. Brewin, S. Ciavatta, Fabm-spectral (2021). doi:http://doi.org/10.5281/zenodo.4594277.

[36] J. Skákala, D. A. Ford, J. Bruggeman, T. Hull, J. Kaiser, R. R. King, B. R. Loveday, M. R. Palmer, T. J. Smyth, C. A. J. Williams, S. Ciavatta, Towards a multi-platform assimilative system for ocean biogeochemistry, Earth and Space Science Open Archive ESSOAr, submitted to JGR-Oceans (2021).

[37] M. J. Lutz, K. Caldeira, R. B. Dunbar, M. J. Behrenfeld, Seasonal rhythms of net primary production and particulate organic carbon flux to depth describe the efficiency of biological pump in the global ocean, Journal of Geophysical Research: Oceans 112 (C10) (2007).

[38] S. A. Henson, J. P. Dunne, J. L. Sarmiento, Decadal variability in north atlantic phytoplankton blooms, Journal of Geophysical Research: Oceans 114 (C4) (2009).

[39] M. J. Behrenfeld, E. S. Boss, Student's tutorial on bloom hypotheses in the context of phytoplankton annual cycles, Global change biology 24 (1) (2018) 55–77.

[40] J. Huisman, P. van Oostveen, F. J. Weissing, Critical depth and critical turbulence: two different mechanisms for the development of phytoplankton blooms, Limnology and oceanography 44 (7) (1999) 1781–1787.

[41] J. J. Waniek, The role of physical forcing in initiation of spring blooms in the northeast atlantic, Journal of Marine Systems 39 (1-2) (2003) 57–82.

[42] A. Ferreira, H. Hátún, F. Counillon, M. Payne, A. Visser, Synoptic-scale analysis of mechanisms driving surface chlorophyll dynamics in the north atlantic, Biogeosciences 12 (11) (2015) 3641–3653.

[43] J. R. Taylor, R. Ferrari, Shutdown of turbulent convection as a new criterion for the onset of spring phytoplankton blooms, Limnology and Oceanography 56 (6) (2011) 2293–2307.

[44] T. J. Smyth, I. Allen, A. Atkinson, J. T. Bruun, R. A. Harmer, R. D. Pingree, C. E. Widdicombe, P. J. Somerfield, Ocean net heat flux influences seasonal to interannual patterns of plankton abundance, PloS one 9 (6) (2014).

[45] D. A. Ford, J. van der Molen, K. Hyder, J. Bacon, R. Barciela, V. Creach, R. McEwan, P. Ruardij, R. Forster, Observing and modelling phytoplankton community structure in the north sea, Biogeosciences 14 (6) (2017) 1419–1444.

[46] J. Skákala, D. Ford, R. J. Brewin, R. McEwan, S. Kay, B. Taylor, L. de Mora, S. Ciavatta, The assimilation of phytoplankton functional types for operational forecasting in the northwest european shelf, Journal of Geophysical Research: Oceans 123 (8) (2018) 5230–5247.

[47] E. O'Dea, R. Furner, S. Wakelin, J. Siddorn, J. While, P. Sykes, R. King, J. Holt, H. Hewitt, The co5 configuration of the 7 km atlantic margin model: large-scale biases and sensitivity to forcing, physics options and vertical resolution, Geoscientific Model Development 10 (8) (2017) 2947.

[48] J. Siddorn, R. Furner, An analytical stretching function that combines the best attributes of geopotential and terrain-following vertical coordinates, Ocean Modelling 66 (2013) 1–13.

[49] D. Storkey, E. Blockley, R. Furner, C. Guiavarc'h, D. Lea, M. Martin, R. Barciela, A. Hines, P. Hyder, J. Siddorn, Forecasting the ocean state using nemo: The new foam system, Journal of operational oceanography 3 (1) (2010) 3–15.

[50] H.-J. Lenhart, D. K. Mills, H. Baretta-Bekker, S. M. Van Leeuwen, J. Van Der Molen, J. W. Baretta, M. Blaas, X. Desmit, W. Kühn, G. Lacroix, et al., Predicting the consequences of nutrient reduction on the eutrophication status of the north sea, Journal of Marine Systems 81 (1-2) (2010) 148–170.

[51] J. Blackford, An analysis of benthic biological dynamics in a north sea ecosystem model, Journal of Sea Research 38 (3-4) (1997) 213–230.

[52] R. Geider, H. MacIntyre, T. Kana, Dynamic model of phytoplankton growth and acclimation: responses of the balanced growth rate and the chlorophyll a: carbon ratio to light, nutrient-limitation and temperature, Marine Ecology Progress Series 148 (1997) 187–200.

[53] J. Baretta-Bekker, J. Baretta, W. Ebenhöh, Microbial dynamics in the marine ecosystem model ersem ii with decoupled carbon assimilation and nutrient uptake, Journal of Sea Research 38 (3-4) (1997) 195–211.

[54] Y. Artioli, J. C. Blackford, M. Butenschön, J. T. Holt, S. L. Wakelin, H. Thomas, A. V. Borges, J. I. Allen, The carbonate system in the north sea: Sensitivity and model validation, Journal of Marine Systems 102 (2012) 1–13.

[55] H. E. Garcia, R. A. Locarnini, T. P. Boyer, J. I. Antonov, O. K. Baranova, M. M. Zweng, J. R. Reagan, D. R. Johnson, A. V. Mishonov, S. Levitus, World ocean atlas 2013. volume 4, dissolved inorganic nutrients (phosphate, nitrate, silicate) (2013).

[56] R. M. Key, A. Olsen, S. van Heuven, S. K. Lauvset, A. Velo, X. Lin, C. Schirnick, A. Kozyr, T. Tanhua, M. Hoppema, et al., Global ocean data analysis project, version 2 (glodapv2) (2015).

[57] S. K. Lauvset, R. M. Key, A. Olsen, S. van Heuven, A. Velo, X. Lin, C. Schirnick, A. Kozyr, T. Tanhua, M. Hoppema, et al., A new global interior ocean mapped climatology: The 1× 1 glodap version 2, Earth System Science Data 8 (2016) 325–340.

[58] Z.-P. Lee, K.-P. Du, R. Arnone, A model for the diffuse attenuation coefficient of downwelling irradiance, Journal of Geophysical Research: Oceans 110 (C2) (2005).

[59] T. J. Smyth, Y. Artioli, Global inherent optical properties from SeaWiFS data (2010). doi:10.1594/PANGAEA.741913.
URL https://doi.org/10.1594/PANGAEA.741913

[60] S. A. Good, M. J. Martin, N. A. Rayner, En4: Quality controlled ocean temperature and salinity profiles and monthly objective analyses with uncertainty estimates, Journal of Geophysical Research: Oceans 118 (12) (2013) 6704–6716.

[61] J. While, M. J. Martin, Variational bias correction of satellite sea-surface temperature data incorporating observations of the bias, Quarterly Journal of the Royal Meteorological Society 145 (723) (2019) 2733–2754.

[62] S. Sathyendranath, R. J. Brewin, C. Brockmann, V. Brotas, B. Calton, A. Chuprin, P. Cipollini, A. B. Couto, J. Dingle, R. Doerffer, et al., An ocean-colour time series for use in climate studies: The experience of the ocean-colour climate change initiative (oc-cci), Sensors 19 (19) (2019) 4285.

[63] J. W. Campbell, The lognormal distribution as a model for bio-optical variability in the sea, Journal of Geophysical Research: Oceans 100 (C7) (1995) 13237–13254.

[64] A. D. Beaton, C. L. Cardwell, R. S. Thomas, V. J. Sieben, F.-E. Legiret, E. M. Waugh, P. J. Statham, M. C. Mowlem, H. Morgan, Lab-on-chip measurement of nitrate and nitrite for in situ analysis of natural waters, Environmental science & technology 46 (17) (2012) 9548–9556.

[65] A. G. Vincent, R. W. Pascal, A. D. Beaton, J. Walk, J. E. Hopkins, E. M. S. Woodward, M. Mowlem, M. C. Lohan, Nitrate drawdown during a shelf sea spring bloom revealed using a novel microfluidic in situ chemical sensor deployed within an autonomous underwater glider, Marine Chemistry 205 (2018) 29–36.

[66] A. Birchill, G. Clinton-Bailey, R. Hanz, E. Mawji, T. Cariou, C. White, S. Ussher, P. Worsfold, E. P. Achterberg, M. Mowlem, Realistic measurement uncertainties for marine macronutrient measurements conducted using gas segmented flow and lab-on-chip techniques, Talanta 200 (2019) 228–235.

[67] I. Hinrichs, V. Gouretski, J. Pätch, K. Emeis, D. Stammer, North sea biogeochemical climatology (2017).

[68] K. Mogensen, M. Balmaseda, A. Weaver, M. Martin, A. Vidard, Nemovar: A variational data assimilation system for the nemo ocean model, ECMWF newsletter 120 (2009) 17–22.

[69] K. Mogensen, M. A. Balmaseda, A. Weaver, et al., The nemovar ocean data assimilation system as implemented in the ecmwf ocean analysis for system 4 (2012).

[70] J. Waters, D. J. Lea, M. J. Martin, I. Mirouze, A. Weaver, J. While, Implementing a variational data assimilation system in an operational 1/4 degree global ocean model, Quarterly Journal of the Royal Meteorological Society 141 (687) (2015) 333–349.

[71] S. Kay, R. McEwan, D. Ford, North west european shelf production centre northwestshelf_analysis_forecast_bio_004_011, quality information document, Copernicus Marine Environment Monitoring Service (2019).

[72] R. R. King, J. While, M. J. Martin, D. J. Lea, B. Lemieux-Dudon, J. Waters, E. O'Dea, Improving the initialisation of the met office operational shelf-seas model, Ocean Modelling 130 (2018) 1–14.

[73] D. Ford, Assimilating synthetic biogeochemical-argo and ocean colour observations into a global ocean model to inform observing system design, Biogeosciences 18 (2) (2021) 509–534.

[74] S. Bloom, L. Takacs, A. Da Silva, D. Ledvina, Data assimilation using incremental analysis updates, Monthly Weather Review 124 (6) (1996) 1256–1271.

[75] H. Sverdrup, On conditions for the vernal blooming of phytoplankton, J. Cons. Int. Explor. Mer 18 (3) (1953) 287–295.

[76] M. Goodliff, T. Bruening, F. Schwichtenberg, X. Li, A. Lindenthal, I. Lorkowski, L. Nerger, Temperature assimilation into a coastal ocean-biogeochemical model: assessment of weakly and strongly coupled data assimilation, Ocean Dynamics 69 (10) (2019) 1217–1237.

Supporting Information for "Improved consistency between the modelling of ocean optics, biogeochemistry and physics, and its impact on the North-West European Shelf seas"

Jozef Skákala[1,2], Jorn Bruggeman[1], David Ford[3], Sarah Wakelin[4], Anıl Akpınar[4], Tom Hull[5,6], Jan Kaiser[6], Benjamin R. Loveday[7], Charlotte A.J. Williams[4]and Stefano Ciavatta[1,2]

[1]Plymouth Marine Laboratory, The Hoe, Plymouth, PL1 3DH United Kingdom.

[2]National Centre for Earth Observation, Plymouth, PL1 3DH, UK.

[3]Met Office, FitzRoy Road, Exeter, EX1 3PB UK.

[4]National Oceanography Centre, Joseph Proudman Building, 6 Brownlow Street, Liverpool, L3 5DA UK.

[5]Centre for Environment, Fisheries and Aquaculture Science, Lowestoft, NR33 0HT UK.

[6]Centre for Ocean and Atmospheric Science, University of East Anglia, Norwich, NR4 7TJ, UK.

[7]Innoflair UG, Richard-Wagner-Weg 35, 64287, Darmstadt, Germany.

Contents of this file

Figures

The panels in the Fig.S1-S10 use the following abbreviations: "free 1-way": free run of the one-way coupled model, "free 2-way": free run of the two-way coupled model, "phys DA 1-way": physical data assimilation into the one-way coupled model, "phys DA 2-way": physical data assimilation into the two-way coupled model, "chl DA 1-way": chlorophyll assimilation into the one-way coupled model, "chl DA 2-way": chlorophyll assimilation

into the two-way coupled model, “phys+chl DA 1-way”: joint physical data - chlorophyll assimilation into the one-way coupled model, “phys+chl DA 2-way”: joint physical data - chlorophyll assimilation into the two-way coupled model.

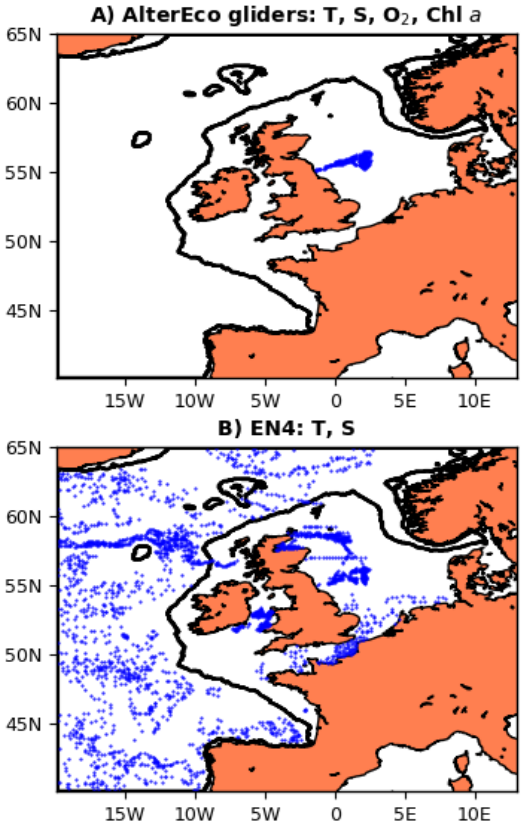

Figure S1. The locations of the 2018 in situ data used both for the assimilation and the validation. The panel A shows the locations of the AlterEco glider measurements and the bottom panel B shows the locations of the EN4 data for temperature and salinity. The EN4 data located outside of the NWE Shelf (bounded by the black line) were used only for assimilation, not for validation.

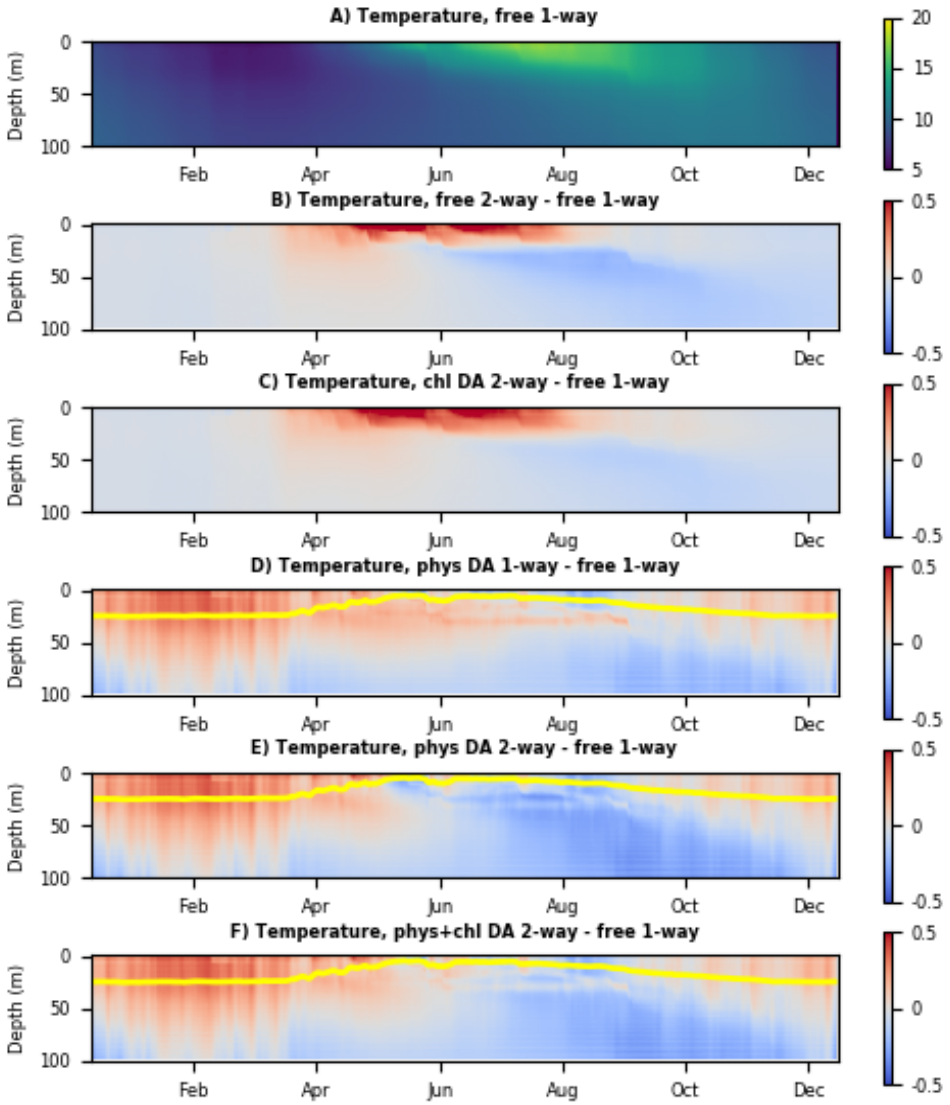

Figure S2. The panel A shows Hovmöller diagram (time on the x-axis vs depth on the y-axis) for the temperature (C) of the one-way coupled free run ("free 1-way"), where the values for each day and depth represent the horizontal spatial averages throughout the NWE Shelf (bathymetry < 200m). Panels B-F show the same Hovmöller diagrams, but for the differences between the two-way coupled, or assimilative runs and the reference, free one-way coupled model run. The purpose of the panels B-F is to provide an understanding of how the bio-optical module and the assimilative model components influence the temperature of the reference free one-way coupled run. The yellow lines in the panels D-F show the MLD of the physical data assimilative runs to indicate the vertical scale of impact of the SST assimilation.

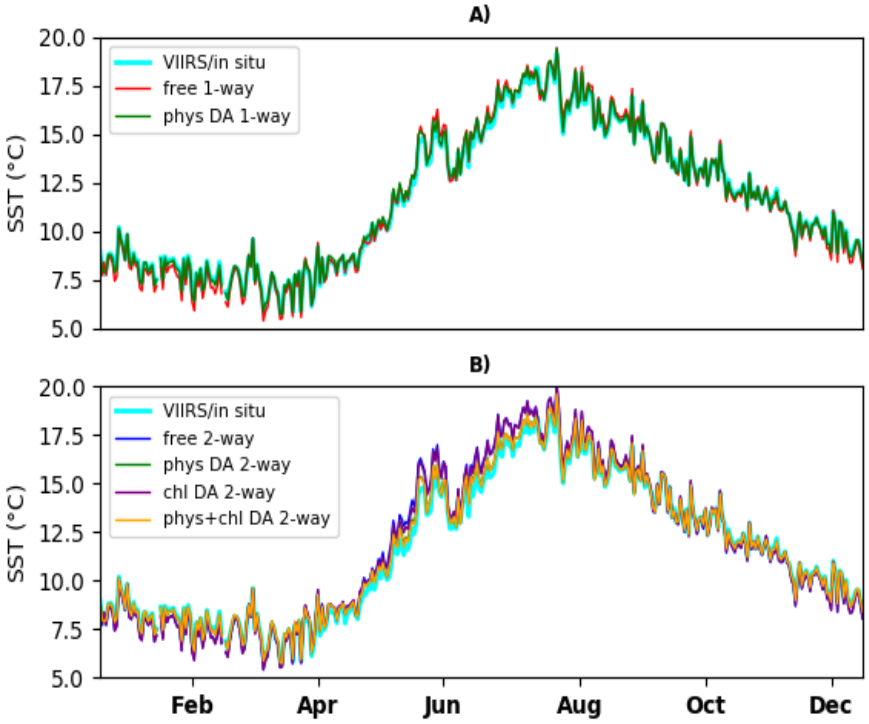

Figure S3. The 2018 time-series of SST averaged throughout the NWE Shelf compared between the different one-way, two-way coupled, free, or assimilative simulations and the VIIRS/in situ data. Panel A compares the different one-way coupled runs, i.e. the one-way coupled free run with the physical data assimilative run, panel B compares the different two-way coupled runs, i.e. the two-way coupled free run with the physical data assimilative run, the chlorophyll assimilative run and the run assimilating both physical data and chlorophyll. To consistently compare the model simulations with the VIIRS/in situ SST, the model outputs were masked wherever there were missing satellite data. The missing satellite data are due to the movements of clouds and atmospheric disturbances and the missing values are responsible for the small time-scale fluctuations in the different curves shown in the three panels. We do not show the one-way coupled runs assimilating chlorophyll, as those have by definition no impact on the simulated temperature.

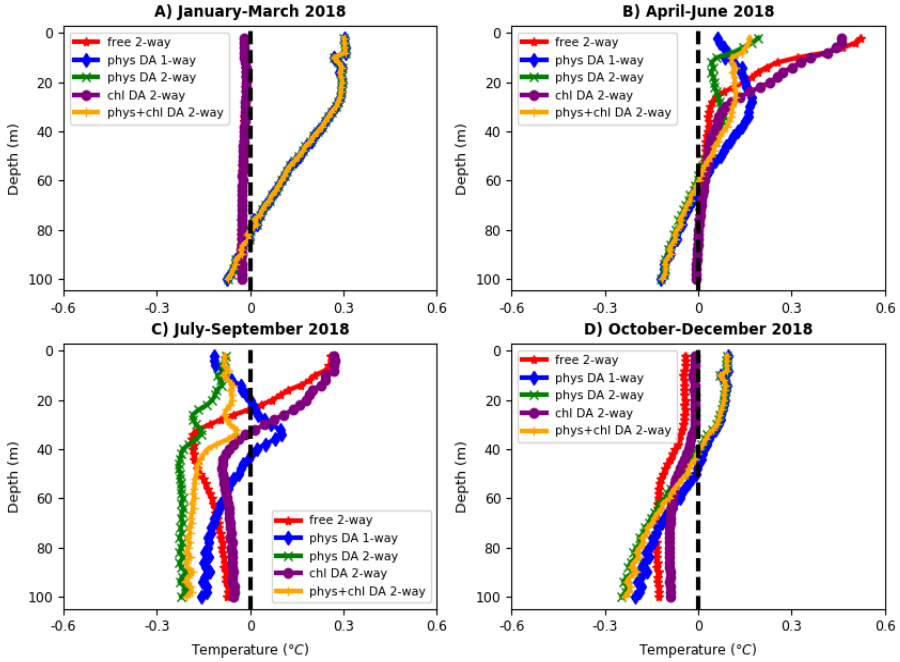

Figure S4. The seasonal differences in temperature (x-axis, °C) between the two-way coupled, or assimilative runs and the reference, one-way coupled free run. The differences are shown as a function of depth (y-axis, m), and averaged throughout the seasonal period and the NWE Shelf.

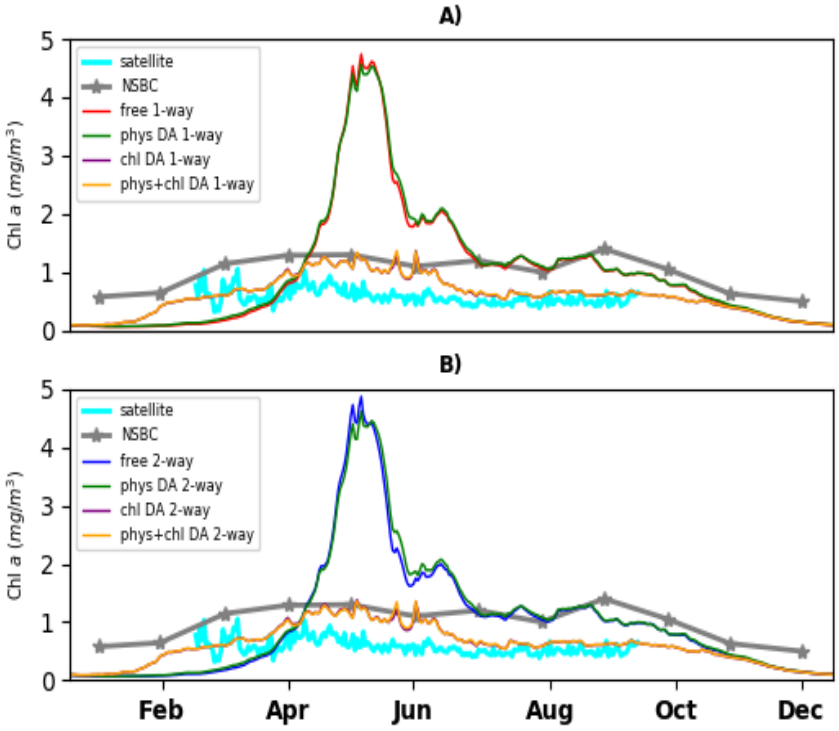

Figure S5. The 2018 time-series of surface chlorophyll a concentrations (mg/m^3) averaged throughout the NWE Shelf compared between the different one-way, two-way coupled, free, or assimilative simulations and the satellite data, as well as with the NSBC climatological data-set. Panel A compares the different one-way coupled runs, i.e. the one-way coupled free run with the physical data assimilative run, the chlorophyll assimilative run and the joint physical data-chlorophyll assimilative run, panel B compares the different two-way coupled runs, i.e. the two-way coupled free run with the physical data assimilative run, the chlorophyll assimilative run and the joint physical data-chlorophyll assimilative run. The chlorophyll assimilative run from both panels A and B is hard to see, as the line is nearly identical with the joint physical-chlorophyll assimilative run. The satellite data were considered only in the March-September period as the data outside this period are scarce and limited only to the southern part of the NWE domain. The small time-scale fluctuations in the satellite data are due to the missing values caused by the movement of clouds and atmospheric disturbances.

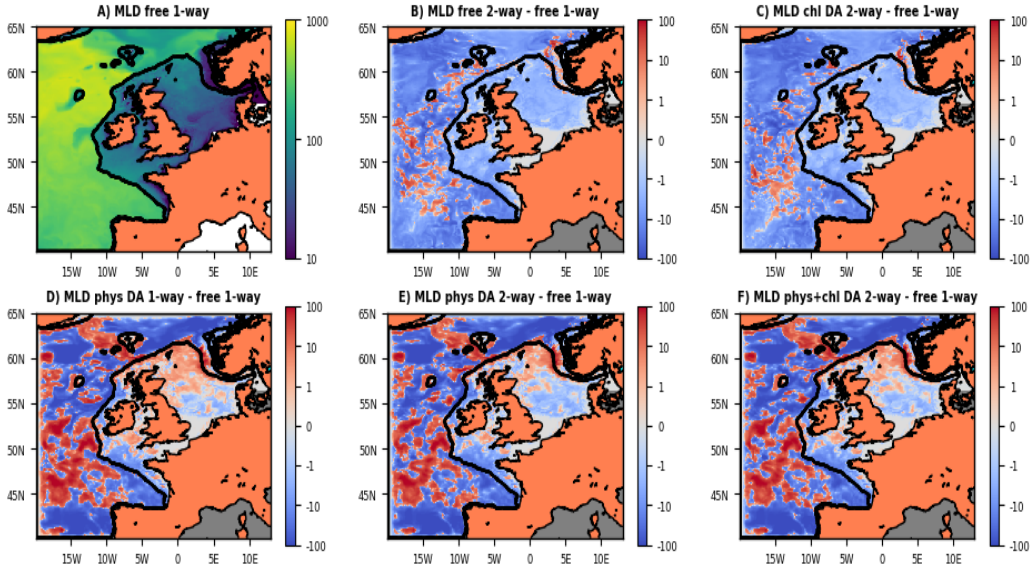

Figure S6. Panel A shows the mixed layer depth (MLD, in m) of the one-way coupled free run (the reference run). The MLD values are averaged for the spring bloom period between March-May 2018. The panels B-F show the relative changes (relative to the one-way coupled free reference run, in m) in MLD carried by the two-way coupled free run (panel B), chlorophyll assimilation into the two-way coupled model (panel C), physical data assimilation into the one-way coupled (panel D) and into the two-way coupled model (panel E) and the joint physical data-chlorophyll assimilation into the two-way coupled model (panel F). All panels B-F show the difference between the MLD of the specific two-way coupled, or assimilative simulation and the one-way coupled free run (panel A). The black line shows the boundary of the continental shelf (bathymetry $<$ 200m).

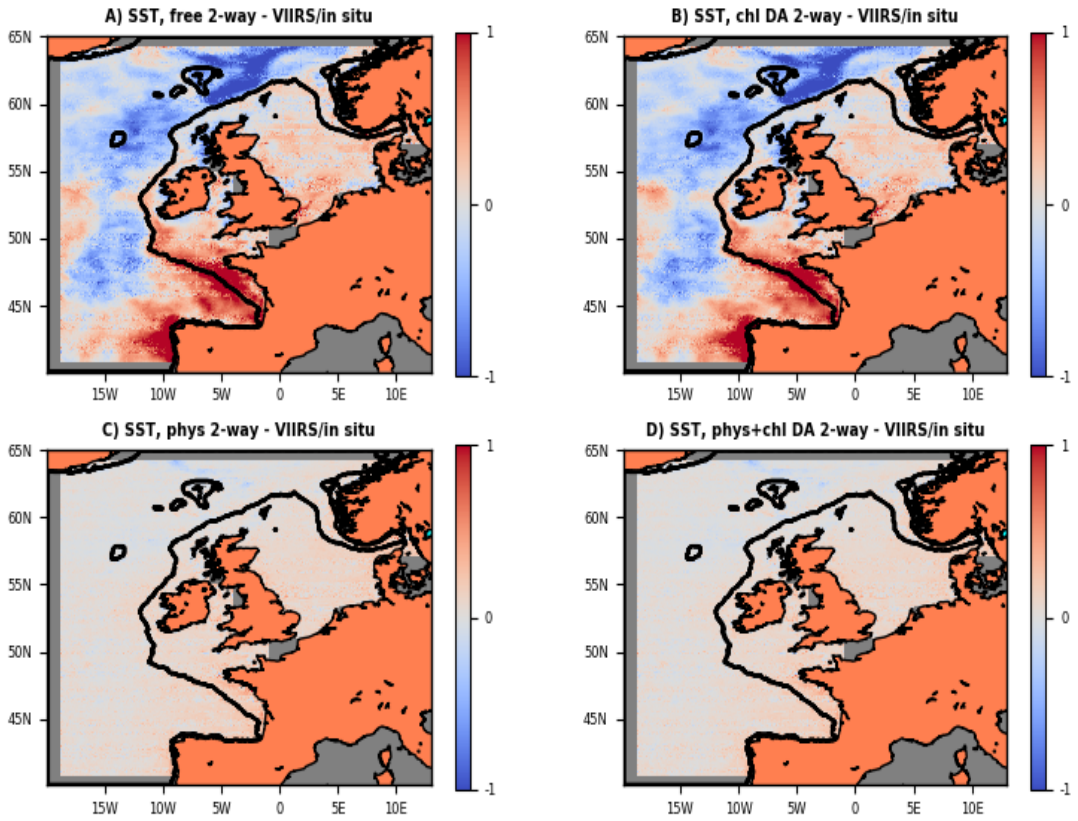

Figure S7. The model to VIIRS/in situ SST differences in °C. The differences are shown for the: free two-way coupled model (panel A), physical data assimilation into the two-way coupled model (panel B), chlorophyll assimilation into the two-way coupled model (panel C), and joint physical data-chlorophyll assimilation into the two-way coupled model (panel D).

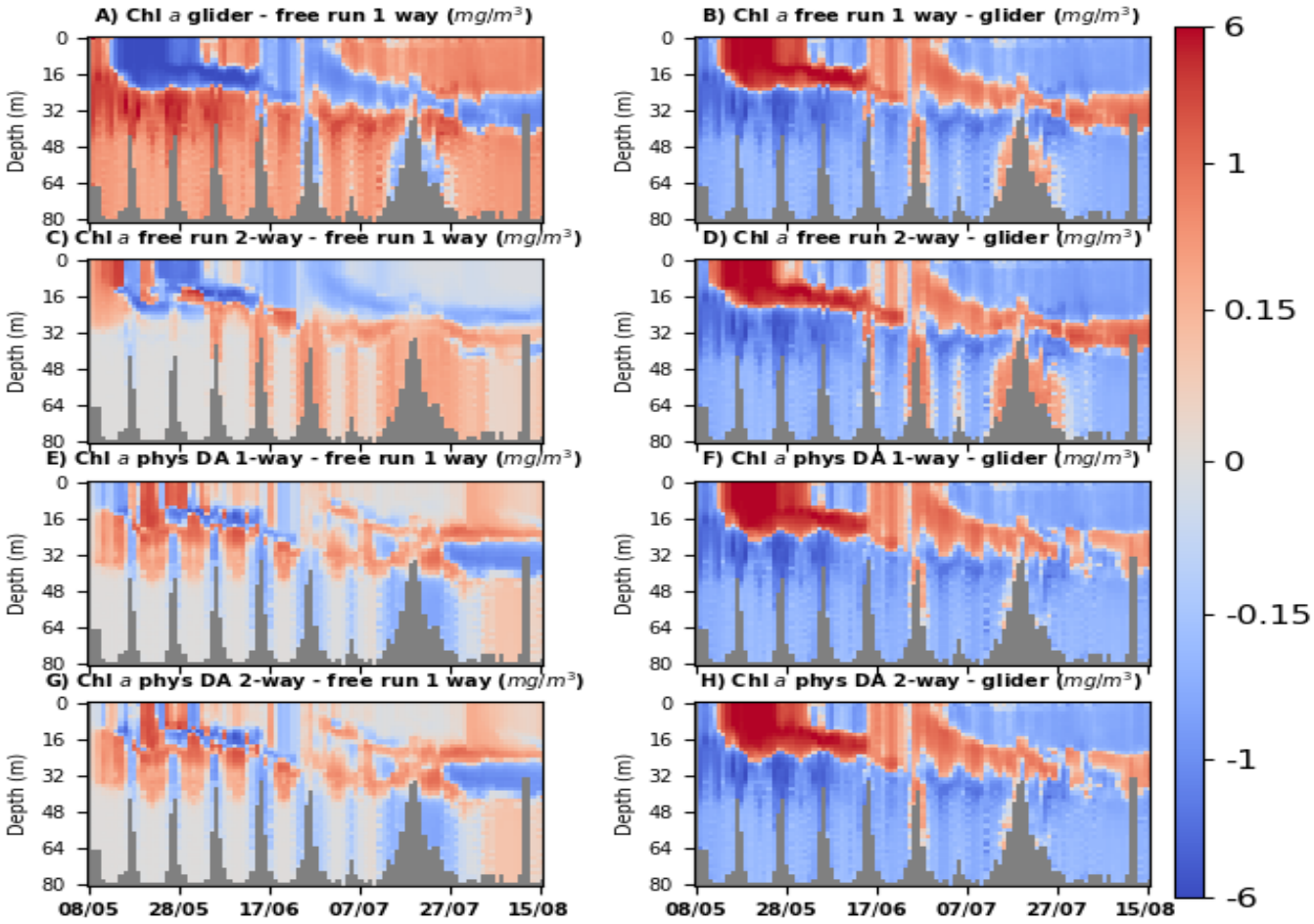

Figure S8. Hovmöller diagram for chlorophyll concentrations (mg/m^3) measured by the Cabot glider in the central North Sea during an early May to mid-August 2018 mission. The right-hand panels (B,D,F,H) show the chlorophyll differences between the free one-way coupled model run (panel B), free two-way coupled model run (panel D), the physical data assimilation into the one-way coupled model (panel F), the physical data assimilation into the two-way coupled model (panel H), and the Cabot glider observations (model minus glider). The left hand panels show the differences between the observations, or model simulations and the reference, free one-way coupled model run. The purpose of the left-hand panels is to show the desired changes to the one-way coupled model (panel A) and how these changes are realized by the biogeochemical feedback in the free run (panel C) and in the physical data-assimilative runs (panels E and G).

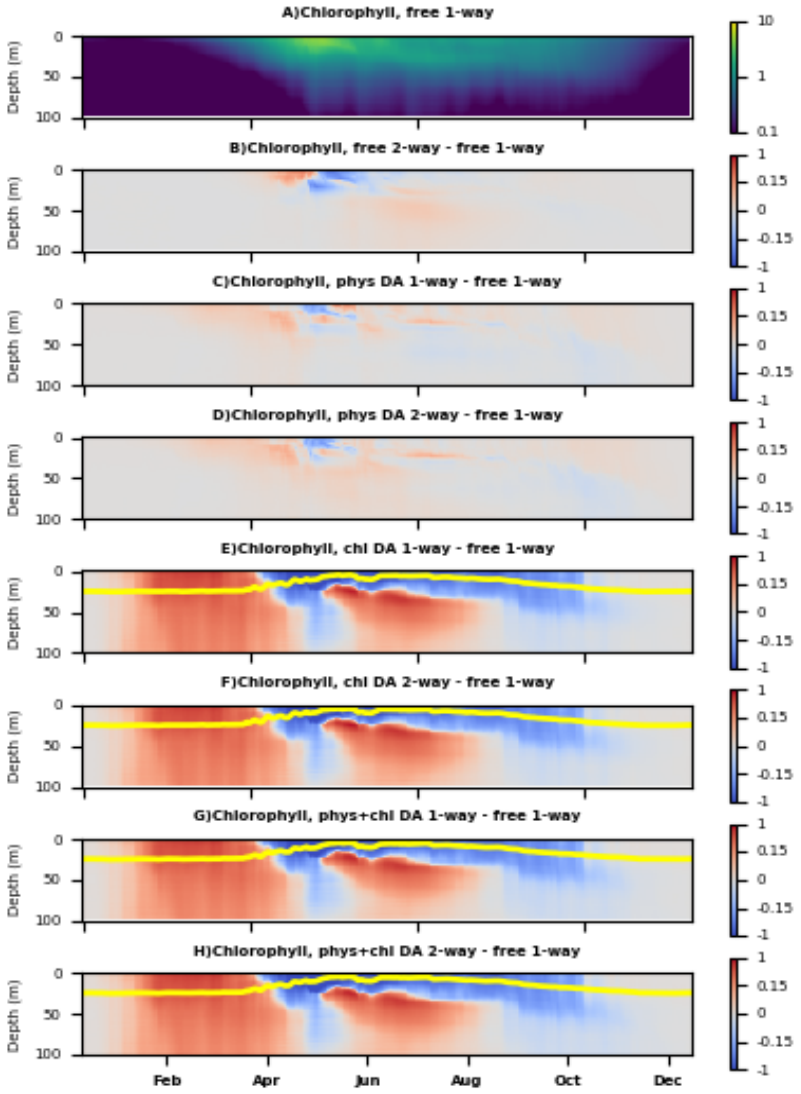

Figure S9. Impact of two-way coupling and assimilation on the simulated chlorophyll concentrations (mg/m^3). The panel A shows Hovmöller diagram (time on the x-axis vs depth on the y-axis) for the one-way coupled model free run, where the values for each day and depth represent the horizontal spatial averages throughout the NWE Shelf (bathymetry $<$ 200m). Panels B-H show the same Hovmöller diagrams, but for the differences between the two-way coupled, or assimilative runs and the reference, free one-way coupled run. The yellow lines in the panels E-H show the mixed layer depth, providing the boundary of the region in which the ocean color assimilation directly updates the simulated chlorophyll.

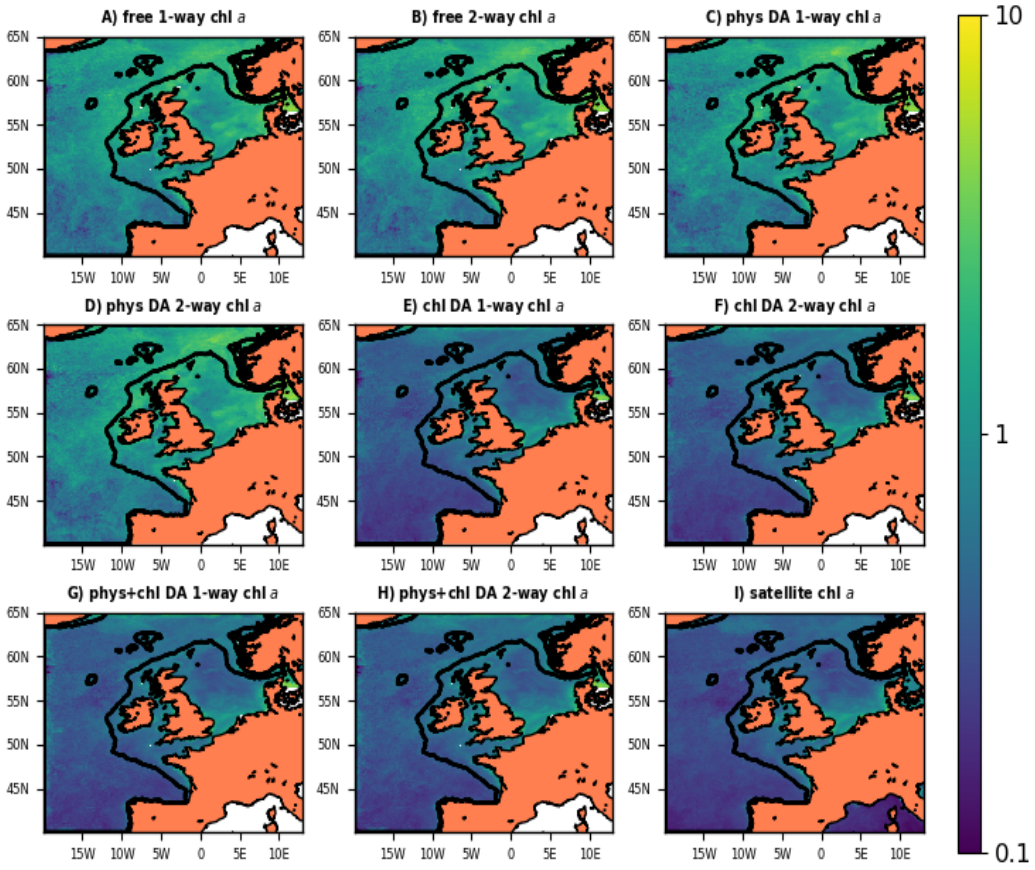

Figure S10. The 2018 mean surface chlorophyll concentrations (in mg/m^3). The different panels compare: the one-way coupled model free run (panel A), the two-way coupled model free run (panel B), the physical data assimilation into the one-way coupled model (panel C), the physical data assimilation into the two-way coupled model (panel D), the chlorophyll assimilation into the one-way coupled model (panel E), the chlorophyll assimilation into the two-way coupled model (panel F), the joint physical data-chlorophyll assimilation into the one-way coupled model (panel G), the joint physical data-chlorophyll assimilation into the two-way coupled model (panel H), and the assimilated satellite ocean color observations (panel I). The black line shows the continental shelf boundary (bathymetry $<$ 200m).